



SHRIMP zircon U–Pb geochronology, elemental, and Nd isotopic geochemistry of the Neoproterozoic mafic dykes in the Yanbian area, SW China

Wei-Guang Zhu^{a,b,*}, Hong Zhong^a, Xian-Hua Li^{b,c}, Hai-Lin Deng^a,
De-Feng He^a, Kong-Wen Wu^a, Zhong-Jie Bai^a

^a State Key Laboratory of Ore Deposit Geochemistry, Institute of Geochemistry, Chinese Academy of Sciences, 46 Guanshui Road, Guiyang 550002, China

^b Key Laboratory of Isotope Geochronology and Geochemistry, Guangzhou Institute of Geochemistry, Chinese Academy of Sciences, Wushan, Guangzhou 510640, China

^c State Key Laboratory of Lithospheric Evolution, Institute of Geology and Geophysics, Chinese Academy of Sciences, Beijing 100029, China

ARTICLE INFO

Article history:

Received 10 July 2007

Received in revised form 25 March 2008

Accepted 26 March 2008

Keywords:

Neoproterozoic
Mafic dykes
Geochemistry
Southwest China
Rodinia

ABSTRACT

Sensitive High-Resolution Ion Microprobe (SHRIMP) U–Pb zircon ages, geochemical and Nd isotopic data are reported for two groups of Neoproterozoic mafic dykes in the Yanbian area of Sichuan Province, SW China. The Group 1 and Group 2 dykes were dated at 792 ± 13 Ma and 761 ± 14 Ma, respectively. While Group 1 and Group 2 rocks are commonly high in Fe_2O_3 and TiO_2 contents with similar MgO contents and Mg numbers, they exhibit distinct trace element features. Group 1 rocks with high $\varepsilon_{\text{Nd}}(T)$ values (+5.8 to +7.2) and total rare earth element (REE) contents (109–171 ppm), are characterized by LREE-enriched and “humped” trace-element patterns with slightly negative Nb–Ta anomaly, similar to typical alkaline basalts associated with continental rifts. Group 2 rocks have relatively low total REE contents (50.4–103 ppm) with relatively flat REE patterns and can be further divided into two sub-types. Group 2a rocks show MORB-like trace element patterns depleted in highly incompatible elements such as Th, Nb, Ta, La and Ce, whereas the Group 2b rocks exhibit flatter REE patterns than those of the Group 2a. The $\varepsilon_{\text{Nd}}(T)$ values of the Group 2a and Group 2b rocks are +5.4 to +7.2 and +4.5 to +5.3, respectively.

The Group 1 and Group 2 dykes display different magma crystallization trends. Group 1 rocks were crystallized from a high-Ti alkaline basaltic magma that was generated by low degrees of partial melting of OIB-like mantle source in the garnet-bearing field. In contrast, the parental magma of Group 2 rocks is similar to those parental to low-Ti tholeiitic basaltic melt generated by relatively higher degrees of partial melting of the asthenospheric mantle source in the spinel-stable field. Group 1 and Group 2a rocks show the intraplate basalts affinity. It is therefore suggested that they originated from an intra-continental rift regime, which was likely related to a mantle plume underneath the supercontinent Rodinia.

© 2008 Elsevier B.V. All rights reserved.

1. Introduction

Proterozoic dyke swarms are important geological time markers that usually punctuate the onset of crustal extension and volcanism (e.g., Zhao and McCulloch, 1993; Zhao et al., 1994). Previous studies of the Neoproterozoic mafic dykes have played important roles in reconstructing the breakup of supercontinent Rodinia in Australia, South China, and western North America (Park et al., 1995; Wingate et al., 1998; Wingate and Giddings, 2000; Z.X. Li et al., 1999; X.H. Li et al., 2006b). The 828 ± 7 Ma mafic to ultramafic dykes and sills in the northern Guangxi Province, South China (Z.X. Li et al., 1999), are identical in age to the 824 ± 4 Ma Amata Dyke Swarm in Central

Australia (Sun and Sheraton, 1996), and to the 827 ± 6 Ma Gairdner Dyke Swarm and 827 ± 9 Ma Little Broken Hill gabbro in southeastern Australia (Wingate et al., 1998). These mafic dykes have been considered to be generated by a Neoproterozoic mantle plume (or mantle superplume) that started continental rifting within Rodinia at ca. 825 Ma (Wingate et al., 1998; Z.X. Li et al., 1999; Wang et al., 2007). The giant radiating dyke swarm, dated at 780 Ma, in three widely separated areas of western North America could also represent the breakup of the supercontinent which included Laurentia and Australia (Park et al., 1995). In addition, the 755 ± 3 Ma Mundine Well Dyke Swarm (MDS) in Western Australia (Wingate and Giddings, 2000; X.H. Li et al., 2006b) and ca. 780–760 Ma dolerite dykes within the Kangding Rift along the western margin of the Yangtze Block (Z.X. Li et al., 2003; Lin et al., 2007) have been suggested to represent the later stage of the Rodinia superplume cycle.

South China, including the Yangtze Block to the northwest and the Cathaysia Block to the southeast, was presumably the central part of the Precambrian supercontinent Rodinia (Z.X. Li et al.,

* Corresponding author at: State Key Laboratory of Ore Deposit Geochemistry, Institute of Geochemistry, Chinese Academy of Sciences, 46 Guanshui Road, Guiyang 550002, China. Tel.: +86 851 5895037; fax: +86 851 5891664.

E-mail address: zhuweiguan@vip.gyig.ac.cn (W.-G. Zhu).

1995). Latest Mesoproterozoic to Neoproterozoic (ca. 1050–740 Ma) igneous rocks are widespread along the western margin of the Yangtze Block. There are two main schools of thoughts regarding the petrogenesis of these igneous rocks. Li and co-authors reported their studies of the volcanic rocks in the Suxiong Group, Kangding–Tongde complexes, Kangding–Shimian mafic dykes, and the metavolcanic rocks in the Yanbian Group in the western margin of the Yangtze Block. It is suggested that the rocks older than 860 Ma (most likely ≥ 900 Ma) rocks were formed prior to or during the Sibao Orogeny associated with the assembly of the supercontinent Rodinia, whereas the 830–740 Ma rocks were anorogenic products related to mantle plume activities during the breakup of Rodinia (X.H. Li et al., 2002a, 2006a; Z.X. Li et al., 2003; Lin et al., 2007). Zhou and others, however, considered that these rocks were formed in a roughly north-south trending (present-day coordinates) active continental margin (Zhou et al., 2002b, 2006a,b; Zhao and Zhou, 2007). Recently, the debate focused on

the mafic–ultramafic complexes and mevolcanic rocks in the Yanbian area (Zhou et al., 2006a, 2007; X.H. Li et al., 2006a, 2007a,b; Munteanu and Yao, 2007; Zhu et al., 2007). Therefore, the petrogenesis and tectonic implications of these igneous rocks are still a matter of hot debate.

Abundant dolerite dykes occurred within the Kangdian Rift along the western margin of the Yangtze Block (Z.X. Li et al., 2003). Field investigations show that these mafic and felsic magmas intermingled with each other in Kangding–Shimian area, implying that the mafic dykes have the same age as the surrounding granites (Z.X. Li et al., 2003; Lin et al., 2007). In addition, there are numerous Neoproterozoic mafic dykes that intruded the Mesoproterozoic to earliest Neoproterozoic and/or the older strata in the Yanbian area (Wang and Kan, 2001; Jiang et al., 2005; Zhu et al., 2006). However, the ages and geochemical characteristics of these mafic dykes have yet been documented, and the petrogenesis of the dykes is not well understood.

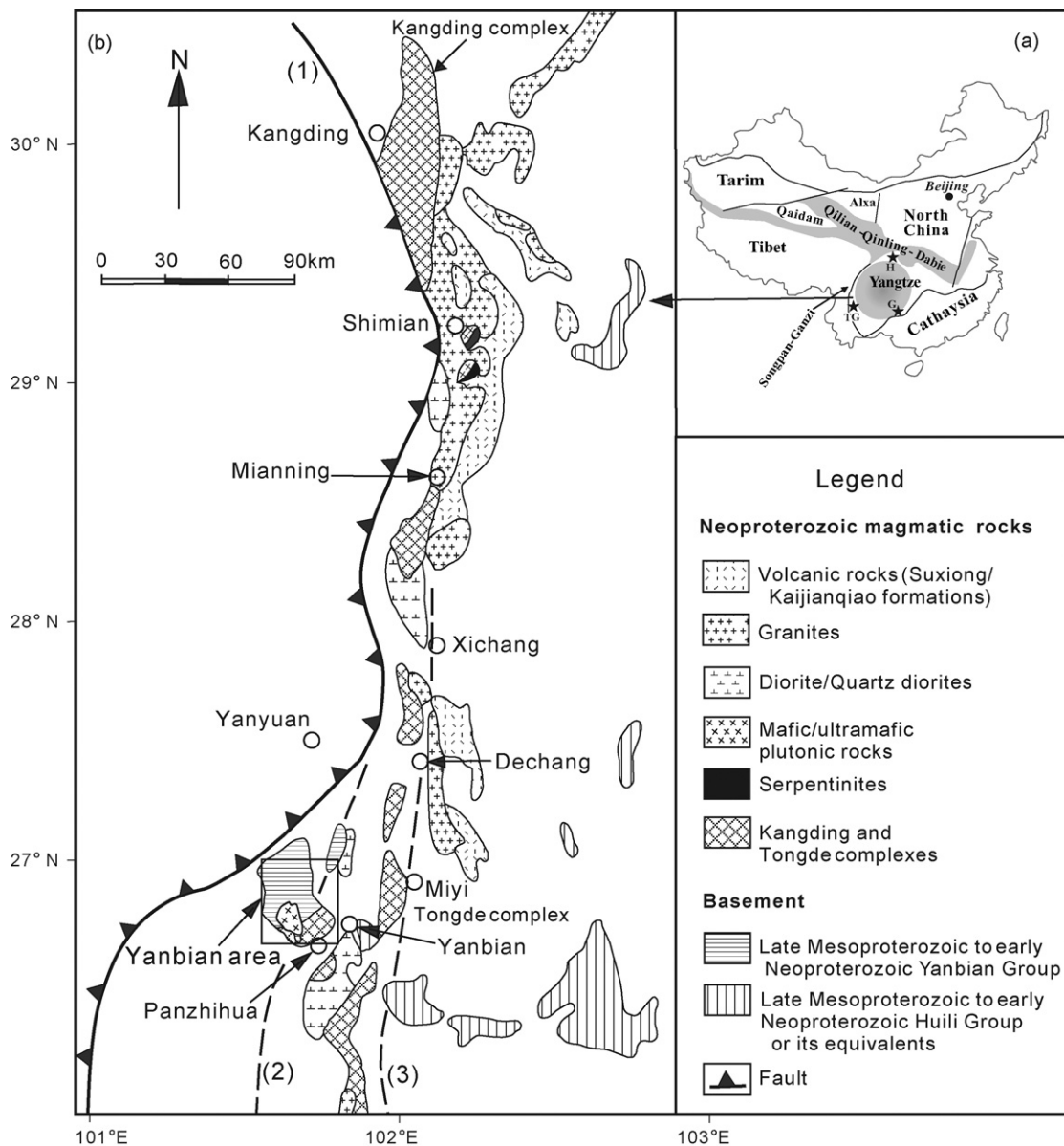


Fig. 1. (a) The location of the Yanbian area in relation to China's major tectonic units. Black stars show the ~830–820 Ma mafic and ultramafic intrusive rocks along the margin of the Yangtze Block. H, Hannan mafic and ultramafic complex (Zhou et al., 2002b; Su et al., 2004); TG, Tongde–Gaojiacun mafic and ultramafic complex (Zhu et al., 2006); G, northern Guangxi mafic dykes and sills (Z.X. Li et al., 1999). (b) Simplified geological map of the Kangding–Panzhihua area, Southwest China, illustrating the Neoproterozoic magmatic rocks and the basement (modified after Sun and Vuagnat, 1992). Symbols: (1), Jinhe–Qinghe fault; (2), Panzhihua fault; (3), Xigeda fault.

In this paper, we report precise Sensitive High-Resolution Ion Microprobe (SHRIMP) U–Pb zircon ages and geochemical and Nd isotopic data for the representative mafic dykes in the Yanbian area with aims to (1) establish the crystallization age for the mafic dykes, (2) constrain the origin and petrogenesis of the mafic rocks, and (3) shed new lights on the Neoproterozoic tectonic evolution along the western margin of the Yangtze Block. Our new results confirm that the mafic dykes in the Yanbian area were derived from two different mantle sources and formed in an intra-continental rift that was most likely induced by the upwelling of a mantle plume underneath the supercontinent Rodinia.

2. Geological background

The Kangding–Panzhuhua area is located in the western margin of the Yangtze Block, to the east of the Songpan–Ganzi orogenic belt (Fig. 1). The basement rocks in this area are mainly composed of late Mesoproterozoic to earliest Neoproterozoic metasedimentary rocks interbedded with felsic and mafic metavolcanic rocks, termed as the Kuyang, Huili and Yanbian Groups (Z.X. Li et al., 2002; X.H. Li et al., 2006a; Greentree et al., 2006). However, no reliable age

constraint is available to test their temporal relationship. These rocks are overlain by a thick sequence (>9 km) of Neoproterozoic (850–540 Ma) to Permian strata composed of clastic, carbonate and metavolcanic rocks. The early Neoproterozoic Suxiong and Kaijianqiao Formations consist of clastic rocks and bimodal volcanic rocks, while the late Neoproterozoic Guanyinya and Dengying Formations comprise clastic rocks in the lower part and phosphorous-bearing carbonate rocks in the upper part (Cong, 1988; SGM, 1991).

Neoproterozoic magmatic rocks are widely distributed in the Kangding–Panzhuhua area, including granites, granodiorites, tonalites, mafic–ultramafic bodies, and mafic dykes (Sinclair, 2001; X.H. Li et al., 2002b, 2003b; Z.X. Li et al., 2003; Shen et al., 2002, 2003; Zhu et al., 2004; Zhou et al., 2002b, 2006a,b; Zhao and Zhou, 2007). These magmatic rocks are well preserved and include, from north to south, the Kangding, Miyi, Datian and Tongde complexes dated at 751–820 Ma (Zhou et al., 2002b; Z.X. Li et al., 2003). These rocks can be generally grouped into two major populations according to their ages, i.e., the older rocks range in age from ca. 830–820 Ma, and the younger rocks in age of ca. 780–750 Ma (X.H. Li et al., 2003b; Z.X. Li et al., 2003). Radiometric ages for the Suxiong/Kaijianqiao Formations range from ca. 815 ± 12 Ma (Rb–Sr

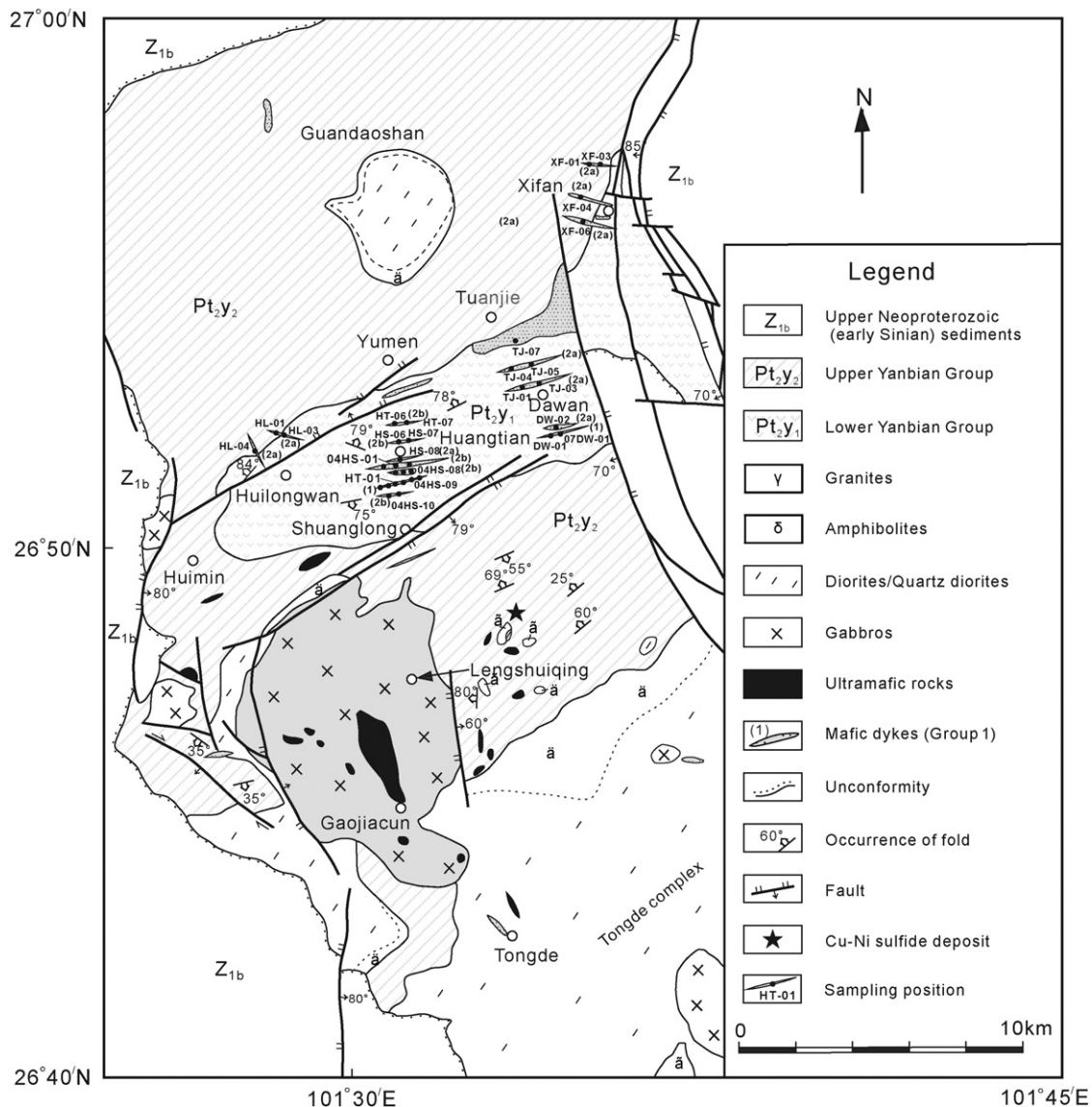


Fig. 2. Simplified Precambrian geological map of the Yanbian area, Sichuan Province, SW China (modified after SBC, 1972).

whole-rock isochron age) in the middle-lower part to 803 ± 12 Ma (SHRIMP zircon U–Pb age) in the middle-upper part of the succession (X.H. Li et al., 2002a). The ages of the Suxiong/Kaijianqiao Formations timed development of the earlier Neoproterozoic continental rift basins in the western margin of the Yangtze Block (Wang and Li, 2003).

There are three major Precambrian rock units in the Yanbian area (Fig. 2): (1) metavolcanic rocks and schists of the late Mesoproterozoic to early Neoproterozoic Yanbian Group, (2) Neoproterozoic igneous bodies that intruded the Yanbian Group, and (3) the Upper Neoproterozoic successions that unconformably overlie the Yanbian Group and some igneous intrusions. The east-west trending Yanbian Group was strongly deformed as well as variably metamorphosed (X.H. Li et al., 2006a; Zhou et al., 2006a) (Fig. 2). The Yanbian Group is divided into four formations: the lower part (Huangtian and Yumen Formations) and the upper part (Xiaoping and Zhaigu

Formations) (SBGMR, 1991). The Huangtian Formation mainly contains metabasaltic pillow lavas, interbedded with several chert and schist layers. The Yumen Formation consists of carbonaceous slate with siltstone in its lower part, and carbonaceous slate and tuffaceous slate in its upper part. The Xiaoping Formation is composed of slate, sandstone and conglomerate. The conglomerates contain clasts of andesite, dacite and rhyolite. The Zhaigu Formation comprises slate and conglomerate (SBG, 1972; SBGMR, 1991).

Neoproterozoic granitoids and mafic–ultramafic intrusive bodies crop out throughout the Yanbian area (Fig. 2). The Guandaoshan dioritic pluton, which intruded the Yanbian Group to the north of the Yumen Township, was emplaced at 857 ± 13 Ma (X.H. Li et al., 2003a). A number of mafic–ultramafic intrusions, including the Tongde gabbro, and the Gaojiacun and Lengshuiqing mafic–ultramafic bodies, also intruded the Yanbian Group (Fig. 2). SHRIMP zircon U–Pb data reveal that the Gaojiacun complex was

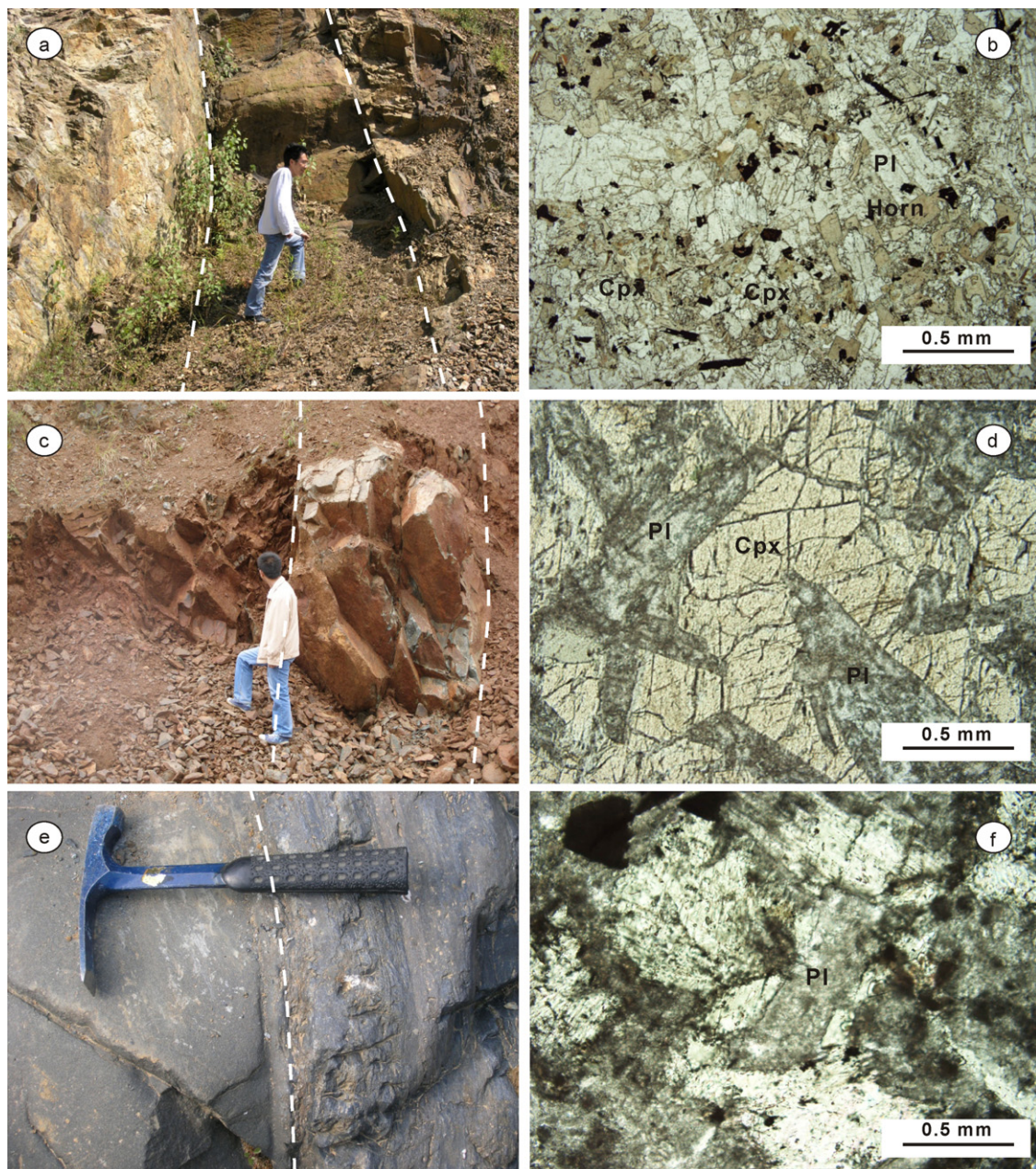


Fig. 3. Field photographs and photomicrographs of the representative mafic dykes: the mafic dykes of the Group 1 (a and b), the Group 2a (c and d), and the Group 2b (e and f).

formed at 825 ± 12 Ma (Zhu et al., 2006). The Lengshuiqing Cu–Ni sulfide-bearing complex, located to the east of the Gaojiacun complex (Fig. 2), has been dated at 821 ± 1 Ma and 813 ± 14 Ma by $^{40}\text{Ar}/^{39}\text{Ar}$ dating of hornblende (Zhu et al., 2007) and SHRIMP U–Pb zircon technique (Zhou et al., 2006a,b), respectively. SHRIMP U–Pb zircon dating also yielded 813 ± 14 Ma and 820 ± 13 Ma for the Tongde diorite and gabbro, respectively (Sinclair, 2001).

The relatively well-preserved mafic dykes in the Yanbian area are exposed to the north of the Gaojiacun and Lengshuiqing complexes, which intruded the metavolcanic rocks and schists of the Yanbian Group (Wang and Kan, 2001; Jiang et al., 2005; Zhu et al., 2006). In the vicinity of the Yumen, Shuanglong, Tuanjie and Dawan localities, the mafic dykes are more abundant than elsewhere in the investigated area. All the dykes were rarely subjected to deformation and metamorphism in contrast to their wall-rocks of the Yanbian Group that were strongly deformed and metamorphosed to greenschist facies (Fig. 3a, c, and e).

The mafic dykes, showing distinctive feature of occurrence, color, rock type, and mineral assemblage, can be divided into two groups (Group 1 and Group 2). Although the cross-cutting relations between the two groups are not observed, both types of dykes exhibit in approximately parallel sets forming swarms near the Huangtian, Shuanglong, Tuanjie and Dawan localities (Fig. 2), implying that they could be nearly coeval. The Group 1 dykes occur exclusively in the lower Yanbian Group to the south of the Huangtian and Dawan villages (Fig. 2). This type of mafic dykes are up to 1 km long and commonly 1–3 m wide, striking NE 70° and dipping to the southeast with an angle of ~ 70 – 85° . Such rocks are relatively fresh to slightly altered, dark-grey to black, fine- to coarse-grained hornblende gabbros, with massive, and sub- to euhedral granular in texture (Fig. 3a and b). Fine-grained chilled margin is usually observed, compared with relatively coarse-grained texture in the interior. These rocks consist of plagioclase (45–65% by volume), clinopyroxene (8–40%), hornblende (8–25%), and subordinate biotite (1%), Fe–Ti oxides (1–2%), apatite and zircon. Electron microprobe analysis indicates that the compositions of pyroxenes from the Group 1 dykes are $\text{Wo}_{37-43}\text{En}_{45-52}\text{Fs}_{10-14}$, belonging to augite (Appendix A). In contrast, numerous Group 2 dykes, composed of variably altered, grey to grey-greenish gabbros and dolerites, intruded the lower and upper Yanbian Group (Fig. 2). They are sub-vertical and comprise a major swarm trending NE 70° to EW, and some trending north-west, with thickness generally ranging from 1 to 5 m (up to 40 m), and the length normally ranging from 1 to 3 km (up to 6 km). These dykes also display obvious fine-grained chilled margins and coarse-grained interiors (Fig. 3c and e). The Group 2 rocks consist mainly of clinopyroxene (48–60%) and plagioclase (40–50%), and minor hornblende (<1%), biotite (<1%), Fe–Ti oxides (<1%). All the rocks underwent variable degrees of saussuritization and epidotization, with the only fresh, sub- to anhedral pyroxenes in thin sections (Fig. 3d and f). The compositions of pyroxenes from the Group 2 dykes are $\text{Wo}_{37-46}\text{En}_{32-42}\text{Fs}_{16-27}$, belonging to augite (Appendix A).

3. Analytical methods

Zircon grains from samples HT-01 and 04HS-01 were separated using conventional heavy liquid and magnetic techniques. Representative zircon grains were handpicked under binocular microscope and mounted in an epoxy resin disc, and then polished and coated with gold film. Zircons were documented with transmitted and reflected light micrographs as well as cathodoluminescence (CL) images to reveal their external and internal structures. The U–Pb isotopic analyses were performed using SHRIMP II at the Chinese Academy of Geological Sciences. Details of the analytical procedures for zircons using SHRIMP can be referred to Compston

et al. (1992) and Song et al. (2002). Inter-element fractionation of ion emission of zircon was corrected relative to the RSES reference TEMORA 1 (417 Ma; Black et al., 2003). The uncertainties in ages are cited as 1σ , and the weighted mean ages are quoted at the 95% confidence interval (2σ).

Chemical compositions of clinopyroxenes were determined by wavelength-dispersion X-ray emission spectrometry using an EPMA-1600 electron microprobe at the State Key Laboratory of Ore Deposit Geochemistry (SKLOG), Institute of Geochemistry, Chinese Academy of Sciences (IGCAS). Major elements were obtained by PANalytical Axios-advance X-ray fluorescence spectrometer (XRF) at SKLOG, IGCAS, using fused lithium-tetraborate glass pellets. Analytical precision as determined on the Chinese National standard GSR-1 was generally around 1–5%. Trace elements were analyzed using a PerkinElmer Sciex ELAN 6000 ICP-MS at the Guangzhou Institute of Geochemistry, CAS. The powdered samples (50 mg) were dissolved in high-pressure Teflon bombs using HF + HNO_3 mixture for 48 h at $\sim 195^\circ\text{C}$ (X.H. Li et al., 2000). Rh was used as an internal standard to monitor signal drift during counting. The international standards GBPG-1, OU-6, and the Chinese National standard GSR-1 were used for analytical quality control. The analytical precision is generally better than 5% for trace elements.

Samples for Nd isotopic analysis were spiked and dissolved in Teflon bombs with HF + HNO_3 acid, and separated by conventional cation-exchange techniques (Zhang et al., 2001). The isotopic measurements were performed on a Finnigan MAT 262 multi-collector mass spectrometer at the Laboratory for Radiogenic Isotope Geochemistry, Institute of Geology and Geophysics, CAS. The measured $^{143}\text{Nd}/^{144}\text{Nd}$ ratios are normalized to $^{146}\text{Nd}/^{144}\text{Nd} = 0.7219$. The $^{143}\text{Nd}/^{144}\text{Nd}$ ratios of the USGS standard rock BCR-1 and La Jolla Nd standard solution determined during this study were 0.512624 ± 11 (2σ), and 0.511852 ± 6 (2σ), respectively.

4. Results

4.1. U–Pb zircon geochronology

Sample HT-01 (N $26^\circ 51.150'$, E $101^\circ 30.979'$) is a hornblende gabbro collected from the Group 1 mafic dykes. Sample 04HS-01 (N $26^\circ 51.409'$, E $101^\circ 30.966'$) is a gabbro collected from the Group 2 mafic dykes (Fig. 2). The SHRIMP zircon U–Pb ages are presented in Table 1.

Zircon grains in sample HT-01 are clear, euhedral prismatic grains with simple internal growth zoning (Fig. 4a). Eighteen analyses from this sample were obtained from 18 grains during a single analytical session. Measured U concentrations vary from 26 to 170 ppm, and Th range from 11 to 161 ppm, with Th/U ratios of 0.27–1.4. Except for spot 15a.1 having obviously older $^{206}\text{Pb}/^{238}\text{U}$ ages of 1076 Ma, possibly due to quite low Th/U ratio and large analytical uncertainties, the remaining 17 analyses constitute two age groups. The older group of eight grains gives an average $^{206}\text{Pb}/^{238}\text{U}$ age of 859 ± 15 Ma (MSWD = 2.4, Fig. 5a). The younger group of nine analyses yield a weighted mean $^{206}\text{Pb}/^{238}\text{U}$ age of 792 ± 13 Ma (MSWD = 1.5, Fig. 5a). Zircons of the older age group are interpreted to be xenocrysts that were identical in age to the ca. 860 Ma Guandaoshan pluton (X.H. Li et al., 2003a), whereas the younger one (792 ± 13 Ma) represents the intrusive age of the Group 1 mafic dykes.

Zircon grains in sample 04HS-01 exhibit simple prismatic igneous shapes and magmatic oscillatory zonings (Fig. 4b). Their U and Th contents vary from 27 to 503 and 17 to 410 ppm, respectively, with Th/U ratios of 0.33–1.7. Apart from two analyses of slightly younger and older grains (5.1 and 8.1) due to large analytical uncertainties, the remainder 10 analyses for this sample yield a mean $^{206}\text{Pb}/^{238}\text{U}$ age of 761 ± 14 Ma (MSWD = 1.02, Fig. 5b). We interpret

Table 1
SHRIMP zircon U–Pb isotopic analyses of the mafic dykes in the Yanbian area, SW China

Spot	U (ppm)	Th (ppm)	Th/U	²⁰⁶ Pb* (ppm)	²⁰⁶ Pb _C (%)	Isotopic ratio					Age (Ma)		
						²⁰⁷ Pb*/ ²⁰⁶ Pb*	±%	²⁰⁷ Pb*/ ²³⁵ U	±%	²⁰⁶ Pb*/ ²³⁸ U	±%	²⁰⁶ Pb*/ ²³⁸ U ± 1σ	²⁰⁷ Pb*/ ²⁰⁶ Pb* ± 1σ
HT-01													
1a.1	100	61	0.62	10.9	0.11	0.0671	2.0	1.179	2.7	0.1274	1.7	770 ± 13	771 ± 13
2a.1	132	116	0.88	15.3	0.12	0.0673	2.0	1.253	2.6	0.1350	1.7	816 ± 13	816 ± 13
3a.1	144	64	0.44	16.6	0.16	0.0698	1.8	1.288	2.4	0.1339	1.6	808 ± 13	806 ± 13
4a.1	37	26	0.70	4.06	0.69	0.0670	3.9	1.174	4.6	0.1272	2.3	768 ± 17	770 ± 18
5a.1	31	28	0.91	3.58	2.86	0.0730	5.7	1.323	6.1	0.1315	2.2	794 ± 19	790 ± 17
6a.1	104	92	0.88	13.3	0.27	0.0758	2.1	1.558	2.7	0.1490	1.7	889 ± 15	888 ± 15
7a.1	75	60	0.80	8.52	0.00	0.0667	2.5	1.212	3.1	0.1319	1.9	798 ± 14	798 ± 15
8a.1	147	161	1.09	18.3	1.17	0.0597	4.2	1.167	4.5	0.1417	1.7	861 ± 14	863 ± 14
9a.1	32	11	0.36	3.51	2.18	0.0581	7.2	1.023	7.6	0.1276	2.5	769 ± 19	781 ± 19
10a.1	111	109	0.98	12.4	0.34	0.0683	3.8	1.224	4.3	0.1299	1.9	786 ± 14	785 ± 14
11a.1	60	42	0.70	6.84	1.58	0.0668	4.1	1.220	4.4	0.1325	1.6	797 ± 13	801 ± 13
12a.1	170	117	0.69	20.7	0.71	0.0616	4.2	1.192	4.3	0.1404	1.1	848 ± 8.9	853 ± 9.3
13a.1	26	18	0.71	3.17	1.41	0.0734	4.4	1.464	4.8	0.1446	1.9	857 ± 17	865 ± 17
14a.1	89	122	1.37	11.5	2.67	0.0664	5.7	1.342	5.8	0.1467	1.1	876 ± 11	885 ± 10
15a.1	67	18	0.27	10.6	0.59	0.0759	2.2	1.913	2.6	0.1827	1.5	1076 ± 15	1081 ± 16
16a.1	77	50	0.64	9.11	0.75	0.0632	3.7	1.192	4.0	0.1368	1.6	825 ± 12	830 ± 13
17a.1	31	25	0.81	3.82	2.48	0.0665	6.3	1.291	6.7	0.1408	2.3	846 ± 20	851 ± 19
18a.1	108	103	0.95	13.3	0.33	0.0654	2.5	1.290	2.6	0.1432	0.95	864 ± 7.7	865 ± 8.1
04HS-01													
1.1	204	345	1.69	21.4	0.16	0.0635	2.5	1.067	4.0	0.1219	3.1	742 ± 22	723 ± 52
2.1	68	47	0.69	7.58	0.28	0.0688	2.2	1.220	3.9	0.1286	3.2	780 ± 24	892 ± 46
3.1	254	297	1.17	28.5	0.12	0.0633	2.9	1.139	4.2	0.1305	3.1	791 ± 23	718 ± 61
4.1	89	57	0.64	9.79	0.13	0.0668	2.2	1.176	3.8	0.1276	3.2	774 ± 23	832 ± 41
5.1	252	410	1.63	22.9	0.24	0.0691	3.1	1.006	4.8	0.1056	3.7	647 ± 23	901 ± 63
6.1	52	17	0.33	5.81	0.61	0.0643	5.7	1.153	6.5	0.1300	3.3	788 ± 24	753 ± 120
7.1	105	55	0.52	11.3	0.00	0.0713	1.7	1.231	3.6	0.1253	3.2	761 ± 23	966 ± 34
8.1	503	291	0.58	58.6	0.00	0.0713	1.1	1.334	3.2	0.1357	3.0	820 ± 23	967 ± 23
9.1	62	30	0.48	6.68	0.35	0.0690	3.1	1.194	4.6	0.1255	3.4	762 ± 25	898 ± 64
10.1	27	17	0.63	2.79	0.00	0.0700	3.7	1.149	5.1	0.1191	3.6	725 ± 24	929 ± 75
11.1	82	48	0.59	8.83	0.00	0.0682	2.3	1.175	4.0	0.1250	3.3	759 ± 24	873 ± 48
12.1	159	164	1.03	16.3	0.10	0.0678	2.3	1.117	3.9	0.1195	3.2	728 ± 22	861 ± 47

Errors are 1σ; ²⁰⁶Pb_C and Pb* indicate the common and radiogenic portions, respectively. Error in standard calibration was 1.29% (not included in above errors but required when comparing data from different mounts). Common Pb corrected using measured ²⁰⁴Pb.

this age as the formation age of the Group 2 rocks, which is slightly younger than that of the Group 1 mafic dykes.

In summary, the dating results indicate that the mafic dykes in the Yanbian area were formed at 790–760 Ma, concurrent with the mafic dykes in the Kangding area (Lin et al., 2007).

4.2. Elemental geochemistry

4.2.1. Alteration effects on chemical compositions

Major and trace element data for the mafic dykes are listed in Table 2. All the samples in this study have undergone variable degrees of alteration, which is shown by relatively high loss-on-ignition (LOI) values of 2.5–7.5%. Thus, the alteration effects on chemical compositions of these rocks need to be evaluated. Zirconium in mafic igneous rocks is generally considered to be the most immobile during low- to medium-grade but severe seafloor-hydrothermal alteration (e.g., Wood et al., 1979; Gibson et al., 1982). A number of elements with different geochemical behaviors, including Nb, Y, Ce, TiO₂, Th, V, Rb, Sr and Ba, are plotted against Zr to evaluate their mobility during alteration (Fig. 6). The high-field strength elements (HFSE: Ti, Y, and Nb), rare earth elements (REEs), Th, and siderophile elements (such as V) correlated tightly with Zr, indicating that these elements are essentially immobile during alteration. In contrast, the low-field strength elements (LFSE: Rb, Sr, and Ba) are overall scattered for the mafic dykes, implying varying degrees of mobility caused by the alteration. Therefore, the sums of their major element oxides are recalculated to 100% volatile free. Meanwhile, only immobile elements are used for geochemical classification and petrogenetic discussions.

4.2.2. Geochemical characteristics of the Group 1 mafic dykes

The Group 1 mafic dykes display high Fe₂O₃ and TiO₂ contents, with SiO₂ = 48.6–51.6% (volatile-free), TiO₂ = 2.1–2.9%, MgO = 7.0–10.4%, Fe₂O₃ = 11.7–14.1%, CaO = 5.6–10.8%, Mg[#] = 51.8–63.9, Cr = 139–637 ppm, and Ni = 80.4–197 ppm (Table 2 and Fig. 7). In the Fenner diagrams (Fig. 7), CaO, Cr, and Ni contents of the Group 1 rocks decrease, whereas SiO₂, Fe₂O₃, TiO₂, Al₂O₃, and P₂O₅ contents increase with decreasing MgO contents. On the plot of Nb/Y vs. Zr/TiO₂ of Winchester and Floyd (1976) (Fig. 8a), rocks from the Group 1 have Nb/Y ratios of 0.72–0.97, plotting exclusively in the alkaline basalt field. On the Ti/Y vs. Nb/Y plot of Peate et al. (1992) and Xu et al. (2001) (Fig. 8b), Group 1 rocks are characterized by high Ti/Y ratios (>500), similar to the high-Ti basaltic rocks.

Group 1 rocks have high total REE contents (REE = 109–171 ppm) with light rare earth element (LREE)-enriched and heavy REE (HREE)-depleted patterns (La_N = 55–89, (La/Yb)_N = 6.7–9.9. Subscript N denotes the chondrite-normalized) (Boynton, 1984) (Fig. 9a), and insignificant Eu anomalies (Eu/Eu* = 0.89–1.1). In the primitive mantle-normalized spider diagram (Sun and McDonough, 1989), the rocks from the Group 1 have “humped” patterns characterized by variable enrichment in all incompatible elements (Fig. 10a). Among them, five samples have negligible Nb–Ta depletion relative to La (Nb/La = 0.86–0.91), resembling typical intraplate alkali basaltic rocks in CFB and OIB provinces (Sun and McDonough, 1989). The others display slightly negative Nb–Ta anomalies relative to La (Nb/La = 0.73–0.83) with relatively high Th abundance, possibly due to crustal contamination.

Table 2
Major element (in wt.%) and trace element (in ppm) data of the mafic dykes in the Yanbian area

	Sample no.											
	04HS-09 1 ^a	HT-01 1 ^a	HT-02 1 ^a	HT-03 1 ^a	HT-04 1 ^a	HT-05 1 ^a	DW-01 1 ^a	07DW-01 1 ^a	XF-01 2a ^a	XF-03 2a ^a	XF-04 2a ^a	XF-06 2a ^a
SiO ₂	48.02	47.10	47.01	49.73	47.36	46.64	47.40	48.38	44.45	44.22	42.49	43.76
TiO ₂	2.57	2.58	2.73	2.04	2.66	2.36	2.03	2.39	2.27	2.36	2.99	2.92
Al ₂ O ₃	12.63	13.63	14.22	14.64	13.79	12.18	12.21	12.26	15.64	15.97	14.30	14.21
Fe ₂ O ₃	12.86	12.50	12.36	11.66	13.69	12.30	11.30	12.29	10.16	11.34	15.52	14.88
MnO	0.34	0.38	0.46	0.52	0.38	0.21	0.16	0.16	0.17	0.18	0.21	0.20
MgO	8.67	6.78	8.53	7.21	8.72	8.83	10.09	8.80	3.75	3.91	7.75	6.97
CaO	9.57	8.74	5.95	5.38	6.91	10.33	10.32	8.93	9.86	9.75	9.27	10.35
Na ₂ O	2.34	3.57	3.32	3.00	2.56	2.11	2.09	2.46	4.10	3.88	2.01	1.89
K ₂ O	1.13	1.06	1.09	1.76	1.10	0.64	0.84	1.12	0.62	0.62	0.14	0.12
P ₂ O ₅	0.25	0.29	0.32	0.39	0.31	0.26	0.23	0.28	0.26	0.26	0.36	0.36
LOI	2.83	3.08	3.31	3.23	2.70	2.63	2.53	2.87	7.52	6.61	4.12	3.57
Total	101.21	99.71	99.31	99.56	100.17	98.49	99.20	99.94	98.81	99.10	99.16	99.23
Mg [#]	57.2	51.8	57.8	55.0	55.8	58.7	63.9	58.7	42.2	40.6	49.7	48.1
Sc	29.6	24.5	23.2	23.2	25.8	28.3	31.5	32.3	39.0	39.6	43.8	42.0
V	319	309	295	228	300	306	238	329	395	403	457	444
Cr	438	221	139	210	227	471	637	547	203	182	327	291
Co	55.4	47.6	67.7	53.7	85.9	58.4	59.1	71.6	66.1	68.4	50.4	51.1
Ni	135	88.6	80.4	104	116	167	197	179	90.6	82.5	72.9	63.5
Cu	113	80.9	80.9	56.7	88.9	107	120	116	75.5	77.9	66.1	58.2
Zn	121	102	76.3	67.2	123	112	95.1	128	102	110	146	131
Ga	18.2	20.1	20.9	18.9	20.8	18.4	16.0	22.5	19.3	19.9	20.0	21.1
Rb	21.8	18.8	21.2	33.4	24.2	11.5	14.5	19.5	13.6	13.5	1.26	1.13
Sr	358	414	388	385	451	423	317	265	215	274	297	367
Y	23.1	25.4	27.1	30.2	27.3	23.6	21.3	29.8	31.8	31.9	40.4	45.7
Zr	189	222	249	234	241	195	162	241	147	147	165	207
Nb	20.7	24.2	26.3	21.9	25.9	21.5	15.5	22.6	4.48	4.54	3.74	4.34
Cs	0.83	0.46	0.44	0.75	1.03	0.77	0.56	0.64	0.41	0.47	0.17	0.12
Ba	421	320	368	590	387	262	256	430	283	274	57.3	58.4
La	24.8	27.4	30.6	29.8	29.6	26.3	17.1	25.3	8.05	7.70	7.36	8.24
Ce	54.3	61.5	64.8	63.9	62.9	56.8	37.8	57.9	22.2	21.6	21.4	24.9
Pr	7.00	7.93	8.45	8.46	8.22	7.33	5.32	7.79	3.53	3.52	3.67	4.08
Nd	32.5	35.7	34.4	35.8	33.8	33.3	25.4	33.7	19.8	19.3	20.7	23.0
Sm	7.10	7.71	7.35	8.04	7.38	7.25	5.75	7.61	5.40	5.61	6.00	7.16
Eu	1.88	2.13	2.40	2.20	2.41	1.90	1.65	2.32	1.81	1.70	2.01	2.19
Gd	5.81	6.24	6.07	7.01	6.27	5.90	4.99	6.92	5.75	5.83	6.93	7.58
Tb	0.86	0.93	0.98	1.08	0.98	0.88	0.75	1.15	0.94	0.95	1.13	1.24
Dy	5.09	5.28	5.50	6.35	5.68	5.20	4.65	5.91	6.10	6.15	7.62	8.31
Ho	0.91	0.99	1.06	1.23	1.07	0.91	0.80	1.20	1.22	1.25	1.52	1.73
Er	2.35	2.63	2.66	3.16	2.75	2.40	2.06	2.87	3.44	3.59	4.24	4.98
Tm	0.32	0.39	0.36	0.44	0.38	0.35	0.30	0.40	0.49	0.52	0.61	0.75
Yb	1.97	2.33	2.09	2.70	2.15	2.03	1.73	2.41	3.21	3.29	3.79	4.68
Lu	0.29	0.31	0.30	0.38	0.30	0.29	0.24	0.33	0.45	0.47	0.59	0.67
Hf	4.48	5.01	6.42	6.38	6.23	4.75	4.00	5.69	3.48	3.56	3.97	4.80
Ta	1.17	1.37	1.63	1.37	1.64	1.19	0.94	1.46	0.26	0.28	0.21	0.28
Pb	3.93	3.06	11.56	7.58	4.53	4.63	2.31	4.53	1.23	1.51	2.35	2.11
Th	3.08	3.73	3.56	4.17	3.51	3.38	2.11	3.05	0.49	0.48	0.26	0.37
U	0.73	0.89	0.85	1.22	0.82	0.80	0.54	0.69	0.19	0.18	0.13	0.15
	Sample no.											
	TJ-01 2a ^a	TJ-03 2a ^a	TJ-04 2a ^a	TJ-05 2a ^a	TJ-07 2a ^a	DW-02 2a ^a	HL-01 2a ^a	HL-03 2a ^a	HL-04 2a ^a	HS-08 2a ^a	HT-06 2b ^a	
SiO ₂	45.95	44.61	46.27	43.21	44.62	45.43	44.87	45.04	44.64	47.08	46.10	
TiO ₂	2.08	2.23	2.20	1.57	2.24	1.65	1.96	2.19	1.95	1.63	2.30	
Al ₂ O ₃	14.81	15.57	15.30	16.55	15.92	16.08	15.97	15.23	15.96	15.51	13.05	
Fe ₂ O ₃	11.74	12.29	11.60	11.31	12.37	11.27	12.29	12.43	12.04	12.13	15.20	
MnO	0.18	0.18	0.17	0.16	0.18	0.16	0.18	0.18	0.19	0.18	0.25	
MgO	6.98	7.27	7.06	9.48	7.24	6.67	7.97	7.23	7.44	7.53	5.32	
CaO	10.32	9.47	9.18	9.48	8.88	8.87	8.18	10.85	9.68	10.21	10.80	
Na ₂ O	3.28	3.25	3.49	2.66	3.37	2.58	3.41	2.89	3.03	2.55	2.64	
K ₂ O	0.38	0.38	0.42	0.15	0.41	0.59	0.25	0.53	0.64	0.32	0.25	
P ₂ O ₅	0.20	0.22	0.22	0.16	0.22	0.20	0.20	0.26	0.20	0.19	0.29	
LOI	3.17	3.36	3.12	4.41	3.35	6.55	3.74	3.01	3.60	3.12	2.54	
Total	99.09	98.83	99.03	99.14	98.80	100.05	99.02	99.84	99.37	100.45	98.74	
Mg [#]	54.1	54.0	54.7	62.4	53.7	54.0	56.2	53.5	55.0	55.2	40.9	
Sc	37.1	38.6	37.8	28.4	38.4	40.5	32.8	36.3	33.5	40.6	42.7	
V	351	371	361	267	359	354	334	384	342	341	466	

Table 2 (Continued)

	Sample no.										
	TJ-01 2a ^a	TJ-03 2a ^a	TJ-04 2a ^a	TJ-05 2a ^a	TJ-07 2a ^a	DW-02 2a ^a	HL-01 2a ^a	HL-03 2a ^a	HL-04 2a ^a	HS-08 2a ^a	HT-06 2b ^a
Cr	170	134	137	133	139	351	152	164	164	267	84.7
Co	44.6	47.8	45.0	54.5	48.6	46.7	56.5	54.5	53.0	38.7	49.8
Ni	61.9	47.2	47.0	118	47.8	87.3	85.8	59.6	81.4	113	33.3
Cu	65.4	64.4	61.3	51.5	61.8	73.3	73.1	82.7	45.4	75.7	73.2
Zn	92.6	99.9	92.2	77.1	96.9	97.6	118	90.5	85.9	104	133
Ga	19.0	20.2	18.0	15.8	19.0	17.6	16.3	18.9	17.7	17.8	20.0
Rb	3.99	4.20	4.50	1.81	4.32	8.99	3.33	7.54	10.4	4.51	6.80
Sr	412	389	378	347	391	248	175	329	337	292	305
Y	27.3	29.3	29.4	18.3	28.8	29.0	25.6	31.3	25.4	28.8	46.3
Zr	136	151	147	94.5	150	91.8	136	166	129	88.4	157
Nb	3.70	4.34	4.11	3.06	4.25	2.25	4.34	5.02	4.36	2.06	4.07
Cs	0.07	0.08	0.07	0.12	0.10	0.52	0.35	0.34	0.41	0.21	1.51
Ba	196	118	153	34.4	85.8	254	131	113	145	144	175
La	6.32	7.17	6.87	5.02	7.31	5.52	6.78	8.06	6.40	5.76	10.7
Ce	18.4	19.8	19.5	13.8	20.5	14.7	19.0	23.0	18.2	15.3	26.6
Pr	2.94	3.26	3.10	2.28	3.39	2.33	3.04	3.86	2.96	2.41	4.12
Nd	15.7	18.0	17.5	12.0	17.7	12.5	16.7	20.2	16.1	12.9	21.6
Sm	4.55	5.13	5.18	3.26	4.91	4.32	4.66	5.55	4.33	3.79	6.26
Eu	1.55	1.61	1.51	1.16	1.60	1.42	1.40	1.57	1.39	1.46	1.93
Gd	5.02	5.40	5.18	3.63	5.26	4.49	4.64	5.47	4.53	4.47	7.11
Tb	0.83	0.88	0.85	0.56	0.87	0.77	0.78	0.94	0.75	0.76	1.20
Dy	5.30	5.72	5.72	3.66	5.77	5.40	5.27	6.00	5.25	5.12	8.44
Ho	1.06	1.15	1.12	0.70	1.13	1.13	1.01	1.23	1.01	1.05	1.79
Er	2.88	3.16	3.19	2.01	3.47	3.28	2.99	3.57	3.00	3.02	5.21
Tm	0.42	0.45	0.44	0.28	0.48	0.48	0.43	0.48	0.43	0.44	0.76
Yb	2.57	2.88	2.96	1.77	2.86	3.08	2.76	3.37	2.76	2.73	4.94
Lu	0.38	0.42	0.41	0.27	0.42	0.48	0.40	0.51	0.39	0.40	0.73
Hf	3.20	3.50	3.57	2.19	3.50	2.30	2.95	3.67	2.90	2.35	3.91
Ta	0.21	0.25	0.24	0.18	0.25	0.13	0.26	0.30	0.26	0.12	0.21
Pb	1.22	0.83	0.93	1.33	1.05	2.51	1.28	1.12	1.22	2.18	2.82
Th	0.26	0.29	0.28	0.18	0.31	0.19	0.32	0.40	0.29	0.17	0.87
U	0.11	0.13	0.14	0.09	0.13	0.07	0.14	0.15	0.15	0.07	0.21
	Sample no.										
	HT-07 2b ^a	HS-06 2b ^a	HS-07 2b ^a	04HS-01 2b ^a	04HS-04 2b ^a	04HS-05 2b ^a	04HS-06 2b ^a	04HS-07 2b ^a	04HS-08 2b ^a	04HS-10 2b ^a	04HS-11 2b ^a
SiO ₂	46.67	46.38	47.16	47.85	46.81	48.40	48.21	48.63	46.65	47.20	46.60
TiO ₂	2.34	2.13	1.95	1.66	2.16	1.69	1.30	1.42	1.51	1.55	1.51
Al ₂ O ₃	13.10	14.17	13.89	14.31	14.42	13.49	14.92	14.88	15.14	15.47	15.02
Fe ₂ O ₃	15.30	14.17	12.71	12.85	14.32	12.80	11.73	11.87	11.86	12.89	12.64
MnO	0.22	0.24	0.19	0.21	0.24	0.19	0.20	0.18	0.19	0.19	0.19
MgO	5.14	6.30	6.85	7.36	6.50	7.75	8.69	7.33	7.25	7.33	7.36
CaO	10.32	10.76	11.27	10.56	9.99	11.09	8.41	8.82	11.11	9.69	10.38
Na ₂ O	2.73	2.87	2.41	2.41	2.98	1.93	3.03	3.30	2.13	2.88	2.36
K ₂ O	0.35	0.12	0.28	0.33	0.16	0.17	0.56	0.19	0.18	0.29	0.47
P ₂ O ₅	0.30	0.24	0.23	0.19	0.27	0.17	0.14	0.17	0.17	0.19	0.17
LOI	2.65	3.28	2.71	2.63	3.00	2.94	3.29	2.90	2.96	3.40	3.47
Total	99.12	100.66	99.65	100.36	100.85	100.62	100.48	99.69	99.15	101.08	100.17
Mg [#]	40.0	46.8	51.6	53.2	47.3	54.5	59.5	55.0	54.8	53.0	53.6
Sc	43.3	47.5	47.9	50.3	49.3	51.7	44.4	35.4	36.6	37.0	37.6
V	473	428	424	353	433	412	268	301	288	291	308
Cr	81.5	252	189	203	238	240	282	170	197	182	185
Co	48.5	51.3	48.2	46.2	51.5	49.6	42.0	40.6	41.4	46.1	43.6
Ni	33.9	80.7	70.3	75.5	72.7	65.0	90.9	64.5	73.8	68.3	66.8
Cu	75.3	89.1	56.5	75.5	95.8	68.5	85.3	31.7	77.8	73.7	93.5
Zn	135	129	99.4	104	127	88.6	74.6	64.2	83.7	103	87.8
Ga	20.6	21.0	18.6	17.5	20.5	17.4	15.3	16.9	18.3	17.3	17.7
Rb	11.3	1.16	3.06	6.02	2.15	2.11	7.39	1.94	2.14	3.06	8.13
Sr	279	467	249	220	437	271	187	226	284	353	315
Y	47.8	41.1	37.4	31.3	42.3	30.6	25.0	24.9	25.6	25.7	24.2
Zr	157	146	127	97.9	149	96.2	74.7	73.2	79.9	73.7	69.9
Nb	4.04	3.44	2.97	2.43	3.23	2.12	1.70	1.68	1.78	1.74	1.69
Cs	2.55	0.22	0.20	0.71	0.33	0.16	0.14	0.13	0.09	0.19	0.29
Ba	241	57.7	127	143	83.1	70.5	148	92.8	59.4	88.5	118
La	10.83	9.63	8.08	7.00	9.54	6.03	5.19	5.79	5.88	6.45	5.63
Ce	26.6	24.0	20.9	17.6	24.2	15.1	13.2	14.7	14.6	15.3	14.2
Pr	4.14	3.77	3.19	2.70	3.72	2.48	2.16	2.35	2.41	2.48	2.29
Nd	22.2	19.4	16.7	14.1	18.6	12.5	11.1	12.0	12.3	12.4	11.6
Sm	6.48	5.30	4.93	4.10	5.70	3.76	3.37	3.41	3.46	3.60	3.43
Eu	1.88	1.91	1.69	1.56	1.85	1.48	1.22	1.24	1.36	1.41	1.32

Table 2 (Continued)

	Sample no.										
	HT-07 2b ^a	HS-06 2b ^a	HS-07 2b ^a	04HS-01 2b ^a	04HS-04 2b ^a	04HS-05 2b ^a	04HS-06 2b ^a	04HS-07 2b ^a	04HS-08 2b ^a	04HS-10 2b ^a	04HS-11 2b ^a
Gd	7.26	6.68	5.81	4.93	6.11	4.67	4.20	4.24	4.35	4.42	4.24
Tb	1.24	1.18	0.97	0.86	1.10	0.83	0.77	0.74	0.77	0.79	0.74
Dy	8.71	7.59	6.77	5.74	7.66	5.32	5.05	4.91	5.07	5.08	4.86
Ho	1.80	1.59	1.46	1.15	1.63	1.12	1.01	0.99	1.09	1.11	1.02
Er	5.27	4.64	4.12	3.26	4.67	3.22	2.98	2.95	3.00	3.05	2.82
Tm	0.76	0.69	0.61	0.47	0.68	0.45	0.43	0.41	0.43	0.45	0.41
Yb	4.90	4.32	3.80	3.04	4.33	2.92	2.84	2.75	2.88	2.87	2.70
Lu	0.74	0.66	0.53	0.45	0.60	0.43	0.42	0.39	0.42	0.42	0.39
Hf	4.05	3.74	3.23	2.62	4.10	2.63	2.18	2.08	2.18	2.15	2.07
Ta	0.22	0.23	0.19	0.16	0.21	0.14	0.12	0.11	0.12	0.12	0.11
Pb	2.71	4.42	1.51	5.41	5.09	4.36	1.06	1.14	1.80	4.35	0.92
Th	0.88	0.67	0.63	0.47	0.71	0.45	0.39	0.38	0.39	0.39	0.38
U	0.23	0.17	0.15	0.13	0.18	0.18	0.09	0.11	0.11	0.13	0.11

Mg[#] = 100 × molar MgO/(Mg + FeO_T), assuming FeO_T = 0.9 × Fe₂O₃. Total iron as FeO_T. LOI = loss on ignition.

^a Group type.

4.2.3. Geochemical characteristics of the Group 2 mafic dykes

In the Nb/Y vs. Zr/TiO₂ diagram (Fig. 8a), rocks from the Group 2 have low Nb/Y ratios (0.07–0.17) plotting into the field of the sub-alkaline basalt. Most of the Group 2 rocks have low Ti/Y ratios (<500; Fig. 8b). On the plot of FeO_T/MgO vs. TiO₂ (Fig. 8c), all the Group 2 samples display the tholeiitic trend. In general, Group 2 rocks show the low-Ti tholeiitic basaltic affinities.

The Group 2 rocks can be further divided into two sub-types (Group 2a and Group 2b) by the trace element characteristics (Figs. 9b and c, and 10b and c). The Group 2a rocks have SiO₂ from 44.7 to 48.7%, TiO₂ from 1.7 to 3.2%, MgO from 4.1 to 10.0%, Fe₂O₃ from 11.1 to 16.3%, CaO from 8.6 to 11.2%, Mg[#] from 40.6 to 62.4, Cr from 133 to 351 ppm, and Ni from 47.0 to 118 ppm. The Group 2b rocks have relatively higher SiO₂ contents (47.6–50.2%) and low TiO₂ contents (1.3–2.4%) than those of the Group 2a rocks. Their MgO contents vary from 5.3 to 8.9%, Fe₂O₃ from 12.1 to 15.9%, CaO from 8.7 to 11.6%, Mg[#] from 40.0 to 59.5, Cr from 81.5 to 282 ppm, and Ni from 33.3 to 90.9 ppm. In the Fenner diagrams (Fig. 7), the Group 2a and Group 2b exhibit similar trends. These rocks increase in SiO₂, Fe₂O₃, TiO₂, CaO, and P₂O₅ with increasing MgO, whereas Al₂O₃, Cr, and Ni decrease.

The Group 2 dykes have relatively low total REE contents (REE = 50.4–103 ppm) with relatively flat REE patterns (Fig. 9b and c). The Group 2a dykes show flat REE patterns with slight depletion in La and Ce (La_N = 16–27, (La/Yb)_N = 1.2–1.9, (La/Sm)_N = 0.72–0.97, (Gd/Yb)_N = 1.2–1.7) and insignificant Eu anomalies (Eu/Eu* = 0.87–1.1). Compared with the Group 2a, rocks from the Group 2b have flat LREE and HREE patterns, with La_N = 17–35, (La/Yb)_N = 1.2–1.5, (La/Sm)_N = 0.97–1.1, (Gd/Yb)_N = 1.1–1.3, and insignificant Eu anomalies (Eu/Eu* = 0.84–1.1). In the primitive mantle-normalized spider diagram, Group 2 rocks are significantly depleted in Th, LREE, Nb, and Ta. Notably, as shown in Fig. 10b and c, Group 2a exhibit N-MORB-like trace element patterns (Sun and McDonough, 1989). The Group 2a has higher Ti contents and Zr/Y ratios, and lower Th and La contents.

4.3. Nd isotopes

Neodymium isotopic data for the mafic dykes are given in Table 3. Group 1 rocks have fairly constant ¹⁴⁷Sm/¹⁴⁴Nd ratios between 0.1289 and 0.1417, ¹⁴³Nd/¹⁴⁴Nd ratios between 0.512593 and 0.512721, corresponding to initial ε_{Nd}(T) values between +5.8 and +7.2. Group 2a and Group 2b have ¹⁴⁷Sm/¹⁴⁴Nd values of 0.1705–0.1883 and 0.1807–0.1899, ¹⁴³Nd/¹⁴⁴Nd values of 0.512842–0.512889 and 0.512789–0.512874, corresponding to

ε_{Nd}(T) values of +5.4 to +7.2 and +4.5 to +5.3, respectively. The Nd isotopic compositions suggest that the parental magmas of the mafic dykes in the Yanbian area were derived from a time-integrated depleted mantle source.

5. Discussion

Although close spatial association of the mafic dykes was observed in the Yanbian area, geochronological data indicate that the two groups of dykes were formed by two distinct magmatic events. Moreover, the obvious differences in petrology and geochemistry between the Group 1 and Group 2 rocks are most likely attributed to their magmatic evolution processes and/or mantle sources.

5.1. Fractional crystallization

The mafic dykes in the Yanbian area exhibit variable MgO concentrations and Mg[#] values, suggesting that they have undergone fractional crystallization to varying degrees. The Group 1 and Group 2 share similar evolutionary trends on some element diagram (Fig. 7). Increase of TiO₂ with decreasing MgO for these rocks indicates that TiO₂ was incompatible in the crystallizing phases and therefore titanomagnetite did not appear liquidus in these systems. The positive correlations of Cr and Ni vs. MgO imply that they may undergo some degrees of fractionation of olivine and/or clinopyroxene.

The positive correlation of Al₂O₃ vs. MgO indicates that the Group 2 mafic dykes were subjected to plagioclase fractionation (Pik et al., 1998), whereas reverse correlations of Al₂O₃ vs. MgO from the Group 1 dykes suggests that they underwent insignificant plagioclase fractionation (Fig. 7). In the CaO vs. MgO diagram (Fig. 7), the Group 1 dykes display an obviously positive correlation, consistent with the removal of Ca-rich mafic phases (e.g., clinopyroxene). In contrast, the Group 2 dykes have relatively constant CaO contents, implying clinopyroxene is not a major fractionated phase for this group.

In summary, olivine and clinopyroxene are the dominated fractionation phases in the Group 1 dykes, whereas plagioclase plus various amounts of olivine and clinopyroxene are the major fractionated minerals for the Group 2 dykes.

5.2. Crustal contamination

The dykes of the Group 1 are enriched in Th and slightly depleted in Nb and Ta (Fig. 10a). Positive correlation between Nb/Th and

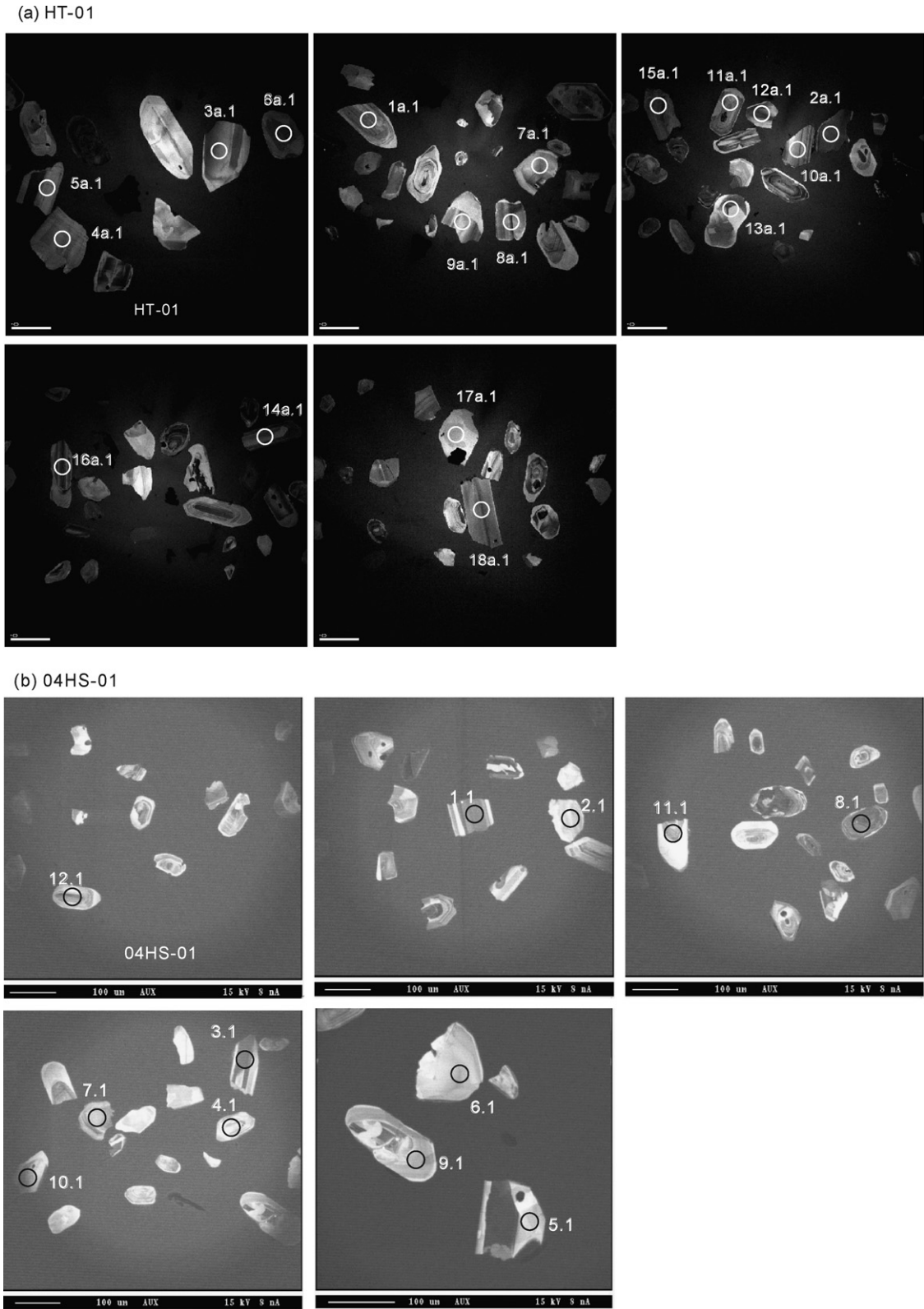


Fig. 4. CL images of zircon grain for sample HT-01 from the Group 1 (a) and sample 04HS-01 from the Group 2 (b) mafic dykes.

Nb/La for the Group 1 dykes (Fig. 11a) suggests involvement of Th-rich components in the magma. Furthermore, their $\epsilon_{Nd}(T)$ values correlate positively with Nb/La (Fig. 11b), but negatively with La/Sm (Fig. 11c), indicating that the relative enrichment of La and

depletion of Nb and Ta in the Group 1 dykes are mostly due to crustal contamination (e.g., Paces and Bell, 1989). In addition, $\epsilon_{Nd}(T)$ values of mafic dykes from the Group 1 decrease with decreasing MgO contents (Fig. 11d), clearly demonstrating they experienced

Table 3
Sm–Nd isotopic compositions of the mafic dykes in the Yanbian area

Sample	Type	Sm (ppm)	Nd (ppm)	$^{147}\text{Sm}/^{144}\text{Nd}$	$^{143}\text{Nd}/^{144}\text{Nd}$	2σ	$(^{143}\text{Nd}/^{144}\text{Nd})_i$	$\varepsilon_{\text{Nd}}(T)$
04HS-09	1	6.810	31.33	0.1314	0.512594	0.000011	0.511913	5.75
HT-01	1	7.612	35.70	0.1289	0.512608	0.000011	0.511941	6.29
HT-05	1	7.142	32.93	0.1311	0.512593	0.000012	0.511914	5.77
DW-01	1	6.072	25.91	0.1417	0.512721	0.000012	0.511987	7.18
XF-03	2a	5.261	18.16	0.1751	0.512842	0.000012	0.511970	6.10
TJ-04	2a	5.049	17.56	0.1738	0.512889	0.000011	0.512023	7.14
TJ-05	2a	3.747	13.29	0.1705	0.512877	0.000012	0.512028	7.24
HL-03	2a	5.822	20.61	0.1707	0.512852	0.000014	0.512001	6.71
HS-08	2a	4.514	14.49	0.1883	0.512873	0.000011	0.511934	5.40
HT-06	2b	7.010	23.46	0.1807	0.512789	0.000010	0.511889	4.52
HS-06	2b	6.271	20.58	0.1842	0.512804	0.000012	0.511886	4.46
04HS-01	2b	4.768	15.37	0.1876	0.512838	0.000013	0.511903	4.79
04HS-06	2b	3.800	12.10	0.1899	0.512874	0.000013	0.511928	5.28
04HS-11	2b	3.750	12.30	0.1843	0.512827	0.000013	0.511909	4.91

Chondrite uniform reservoir (CHUR) values ($^{147}\text{Sm}/^{144}\text{Nd} = 0.1967$, $^{143}\text{Nd}/^{144}\text{Nd} = 0.512638$) are used for the calculation. $\lambda_{\text{Sm}} = 6.54 \times 10^{-12} \text{ year}^{-1}$ (Lugmair and Hart, 1978). The $(^{143}\text{Nd}/^{144}\text{Nd})_i$, $\varepsilon_{\text{Nd}}(T)$ of the Group 1 and Group 2 mafic dykes in the Yanbian area were calculated using age of 790 Ma and 760 Ma, respectively.

crustal assimilation and fractional crystallization processes. In view of these geochemical and isotopic correlations, the crustal contaminants may be main factors causing low in $\varepsilon_{\text{Nd}}(T)$, Nb/La, Nb/Th and MgO, but high in La/Sm, indicative of sialic crust components. Continental crust is typically depleted in Nb and Ta (Rudnick and Fountain, 1995), and the upper continental crust is enriched in La and Th while the lower continental crust is not usually enriched in Th (Barth et al., 2000). As a result, the crustal contaminant enriched in Th and La and depletion in Nb and Ta was possibly derived from the upper crust rather than the lower crust (Fig. 12a) (Ingle et al., 2002). It is therefore suggested that the magmas parental to the Group 1 rocks assimilated relatively high-evolved upper continental crust.

In contrast, a positive correlation between $\varepsilon_{\text{Nd}}(T)$ and MgO for the Group 2 rocks (Fig. 11d) reveals that crustal assimilation and fractional crystallization processes play an important role during their generation. Group 2a and Group 2b rocks display the same magma evolution trend and have similar ratios of Zr/Nb, Ce/Y, (Gd/Yb)_N, and (La/Yb)_N (Fig. 12b–d), implying that they were likely generated by a common primary magma. The samples from the Group 2b, however, exhibit relatively higher Th and La contents, and lower Ti contents and $\varepsilon_{\text{Nd}}(T)$ values than those of the Group 2a samples (Fig. 10b and c, and Table 3). As shown in the Nb/Th–Nb/La (Fig. 11a), $\varepsilon_{\text{Nd}}(T)$ –Nb/La (Fig. 11b), and $\varepsilon_{\text{Nd}}(T)$ –La/Sm (Fig. 11c) diagrams, the less-contaminated rocks from the Group 2a have relatively high Nb and low La contents, whereas the more contaminated rocks from the Group 2b have relatively low Nb and high Th and La contents. The (Th/Ta)_{PM} and (Ta/La)_{PM} relationship (Fig. 12a) indicates that the Group 2 rocks follow a mixing trend between mantle melts and upper continental crust (Ingle et al., 2002). Thus, Group 2a and Group 2b rocks were probably generated from a common primary magma, with involvement of more upper crustal material into the Group 2b rocks.

A quantitative modeling based on the Nb/La ratios and Nd isotopic compositions was conducted by using a binary mixing model. We choose the metasedimentary rocks from the Huili Group, which is similar in composition to the Yanbian Group, as the crustal contaminant (our unpublished data). Sample DW-01 has the highest MgO (10.4%), Ni (197 ppm) and Cr (637 ppm) contents and $\varepsilon_{\text{Nd}}(T)$ value (7.2) in the Group 1, representing the least-contaminated composition of this group. Sample TJ-05 with the highest MgO (10.0%) and $\varepsilon_{\text{Nd}}(T)$ value (7.2) in the Group 2 represents the least-contaminated basaltic rock of Group 2 (Tables 2 and 3). Furthermore, sample DW-01 resembles typical OIB features, whereas

sample TJ-05 is similar to N-MORB-like trace element patterns (Figs. 9 and 10). Thus, the least-contaminated alkaline basalt in the Suxiong volcanics (X.H. Li et al., 2002a) was used to approximate the Group 1 primary magma. The least-contaminated mafic dykes exhibiting N-MORB-like features in the Kangding–Shimian area (Lin et al., 2007) were used to approximate the Group 2 primary magma. As shown in Fig. 13, the modeling results suggest incorporation of minor amount of crustal material (3–8%) into the primary melt parental to the Group 1 mafic dykes, whereas 1–2% and 4–6% crustal contaminant were involved in the generation of the Group 2a and Group 2b rocks, respectively.

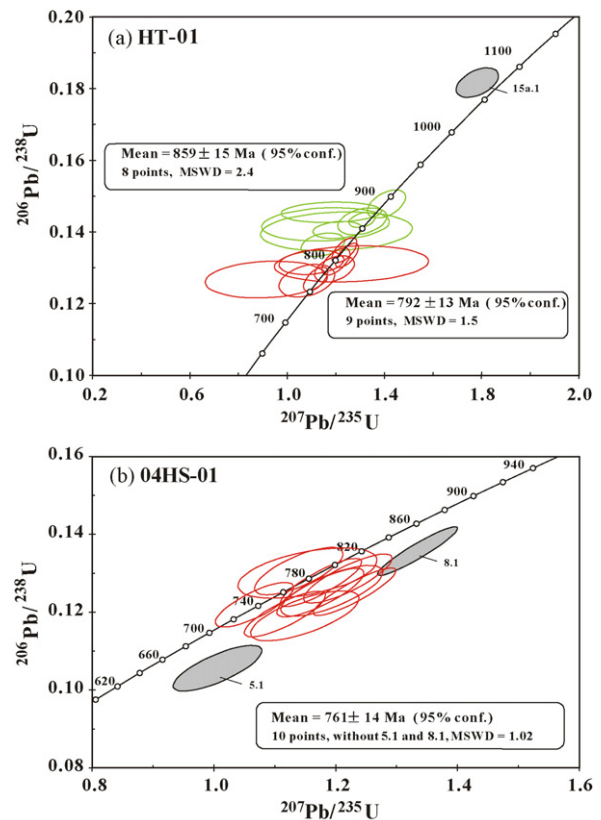


Fig. 5. SHRIMP zircon U–Pb concordia diagrams for sample HT-01 from the Group 1 (a) and sample 04HS-01 from the Group 2 (b) mafic dykes.

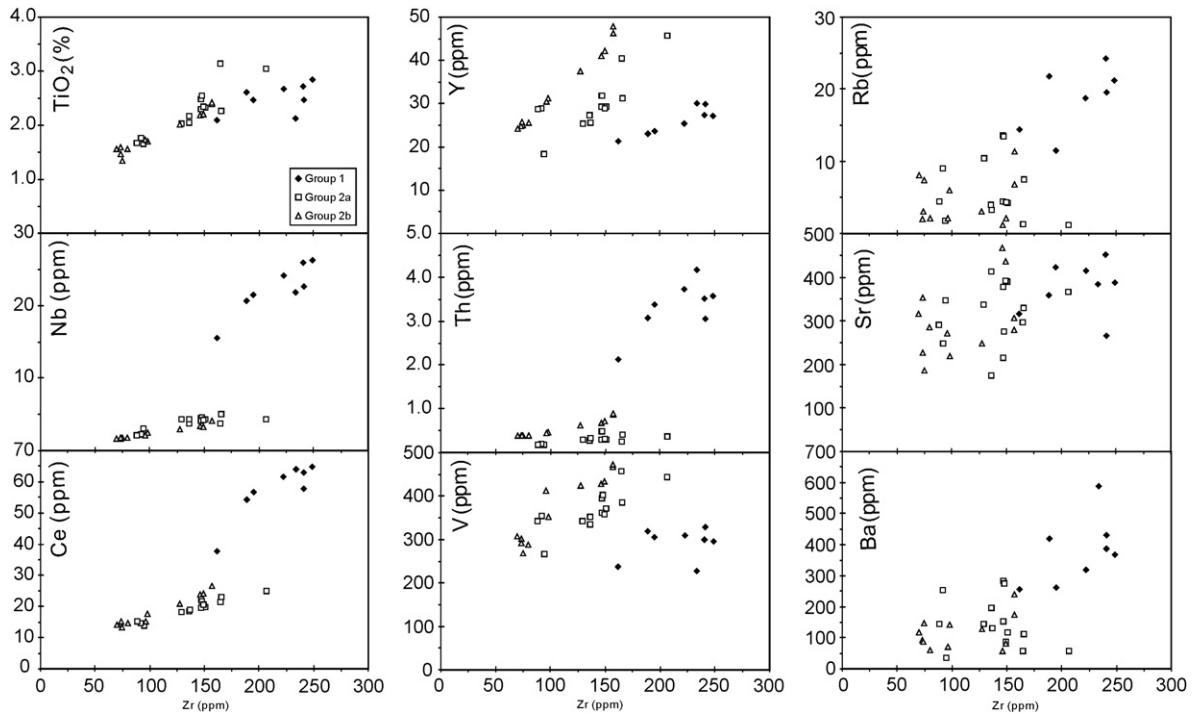


Fig. 6. Plots of TiO_2 , Nb, Ce, Y, Th, V, Rb, Sr, and Ba vs. Zr to evaluate the mobility of these elements of different geochemical behavior during alternation. Solid diamond symbols: the Group 1 mafic dykes; open square symbols: the Group 2a mafic dykes; open triangle symbols: the Group 2b mafic dykes.

As discussed above, these elemental and isotopic characteristics indicate that the parental magmas of these mafic dykes had experienced variable degrees of crustal contamination.

5.3. Nature of the parental magma and mantle source characteristics

An obvious contrast is shown between the Group 1 and Group 2 rocks in terms of their trace element and REE geochemical characteristics (Figs. 9, 10 and 12a). These two groups define two distinct geochemical trends on the Fig. 12b and c, which may be caused by partial melting of the same mantle source with variable melting degrees, or of different mantle sources. The ratios of incompatible elements with similar distribution coefficients are the least susceptible to partial melting and fractional crystallization processes (Wang et al., 2004). The less-contaminated rocks of the Group 1 and Group 2 exhibit obviously different Nb/Th, Nb/La, Zr/Nb ratios (Figs. 11a and b, and 12c), arguing against a scenario that they were generated by variable degrees of partial melting of the same mantle source. Instead we suggest that they originated from two different mantle sources.

5.3.1. Nature and origin of the parental magma of the mafic dykes of Group 1

As shown above, the mafic dykes from Group 1 exhibit the high-Ti alkaline basaltic feature (Fig. 8). In order to minimize the effects of fractionation and crustal contamination, the least-contaminated sample DW-01 of the Group 1 has been modeled using an olivine-addition method to extrapolate the composition of the parental magma (Wang et al., 2002). Equilibrium olivine is added in 1% increments until the resulting basaltic magma is in equilibrium with Fo_{89} olivine, using $K_d = 0.31$, where K_d is the molar ratio of FeO/MgO in olivine to that in the coexisting magma (Roeder and Emslie, 1970), and assuming $\text{Fe}^{2+}/\text{total Fe} = 0.85$. After removing effect of 11% olivine crystallization, the result is a high magnesium magma

containing $\text{SiO}_2 = 48.7\%$, $\text{MgO} = 14.4\%$, and $\text{FeO} = 10.3\%$. Accordingly, it suggests that the parental magma for the Group 1 is a high-Ti and Mg alkaline basaltic magma.

The mafic dykes from Group 1 display high TiO_2 contents, low La/Nb (1.1–1.4) and La/Ta ratios (21–22), and high ratios of Zr/Y (7.6–9.2) and Ti/Y (421–677), similar to those of OIB (La/Nb < 1.5, La/Ta < 22, Zr/Y > 6, and Ti/Y > 410) (Lightfoot et al., 1993; Ewart et al., 1998; Garland et al., 1996; Sun and McDonough, 1989). Moreover, as shown in Fig. 10, the geochemical and Nd isotopic characteristics of the less-contaminated rocks are similar to those of the alkali basalts derived from OIB-like mantle sources in continental rifts, such as alkaline basalts in the modern East African Rift (Stewart and Rogers, 1996; Pik et al., 1999) and ~803 Ma Suxiong alkaline basalts in the Kangding Rift in South China (X.H. Li et al., 2002a). The above discussions reveal that the parental magma of the Group 1 rocks was generated by melting of OIB-like mantle source and most likely triggered by an intra-continental rifting.

It has been proposed that alkali-rich basaltic magma displaying an LREE-enriched pattern may be generated by small degrees of melting of mantle peridotite (Cullers and Graf, 1984; Hirschmann et al., 1998). In general, low La/Yb ratios reflect a melting regime dominated by relatively large melt fractions and/or spinel as the predominant residual phase, whereas high La/Yb ratios are indicative of smaller melt fractions and/or garnet control (Deniel, 1998; Xu et al., 2001). In addition, REE fractionation, presented on a plot of La/Yb vs. Tb/Yb (Fig. 14), can be used to estimate the nature of mantle source and the extent of melting (George and Rogers, 2002). Superimposed on this diagram is a grid for fractional melts derived from peridotite with REE abundances equivalent to primitive mantle (Sun and McDonough, 1989). Modal garnet in the mantle source region varies from 0 to 8% (subhorizontal lines), representing the total range of modal garnet across the spinel–garnet peridotite transition (Wood and Blundy, 1997). The Group 1 mafic dykes define a steep trend, which is unlikely to be the effect of crustal con-

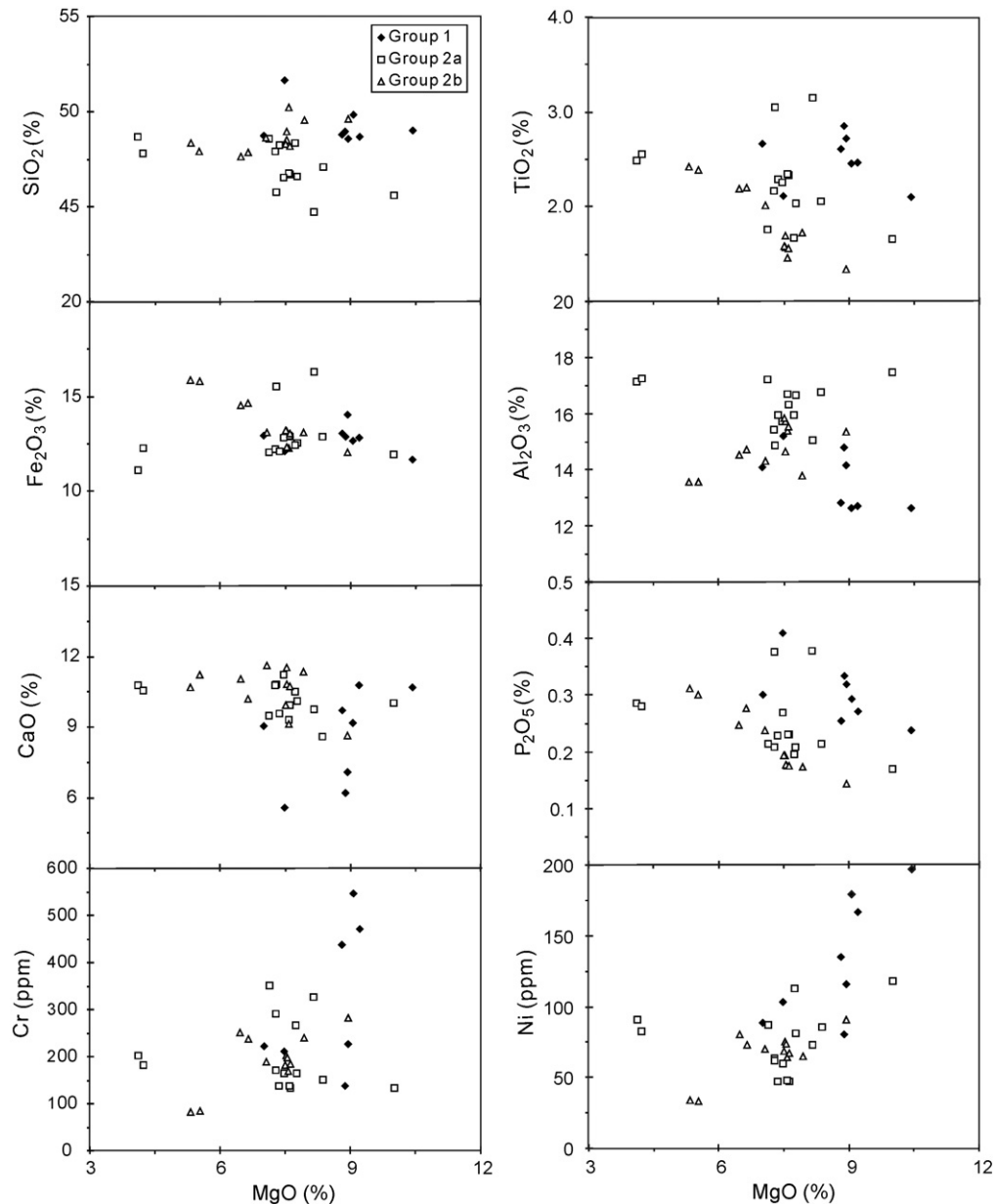


Fig. 7. Fenner diagrams for the mafic dykes in the Yanbian area. Symbols as in Fig. 6.

tamination because such processes have little effect on REE ratios (Thirlwall et al., 1994), and thereby imply variable residual garnet during melting. The highest Tb/Yb ratios indicate that the residual garnet was 1–2%. Melting thus appears to have occurred in the spinel–garnet transition field for the Group 1 rocks. The REE model refers to a melt fractions of ~2.5–3% for the Group 1 rocks.

Therefore, the Group 1 dykes having high La/Yb and Tb/Yb ratios with relatively low HREE abundance were possibly generated by low (~2.5–3%) degree partial melting of a garnet-bearing asthenospheric mantle source.

5.3.2. Nature and origin of the parental magma of the mafic dykes of Group 2

Group 2 mafic dykes display the low-Ti tholeiitic basaltic affinity (Fig. 8). The least-contaminated sample of this group (TJ-05) is selected for calculation of parental magma composition also using an olivine-addition method (Wang et al., 2002). After removing

effect of 16% olivine crystallization, the final result is a high-Mg basaltic melt containing ~45.4% SiO₂, 15.6% MgO, and 11.0% FeO. As a result, the magma parental to the Group 2 is a low-Ti and high-Mg tholeiitic basaltic magma.

Group 2 dykes are characterized by MORB-like elemental pattern with depletions in highly incompatible elements such as Th, Nb, Ta, La, and Ce. However, they are different from typical MORB because (1) the Group 2 have generally higher trace element abundances than typical N-MORB (Figs. 9b and 10b); (2) the magma parental to the Group 2 rocks had been assimilated by silicic crust which are low in $\epsilon_{Nd}(T)$, Nb/La, Nb/Th, and MgO, but high in La/Sm (Fig. 11a–d). This makes it unlikely that the rocks of the Group 2 were formed in an oceanic setting where silicic crust is normally absent.

The Group 2 dykes display a MORB-like elemental pattern, implying that they were most likely derived from a depleted asthenospheric mantle source. In addition, this group dykes are

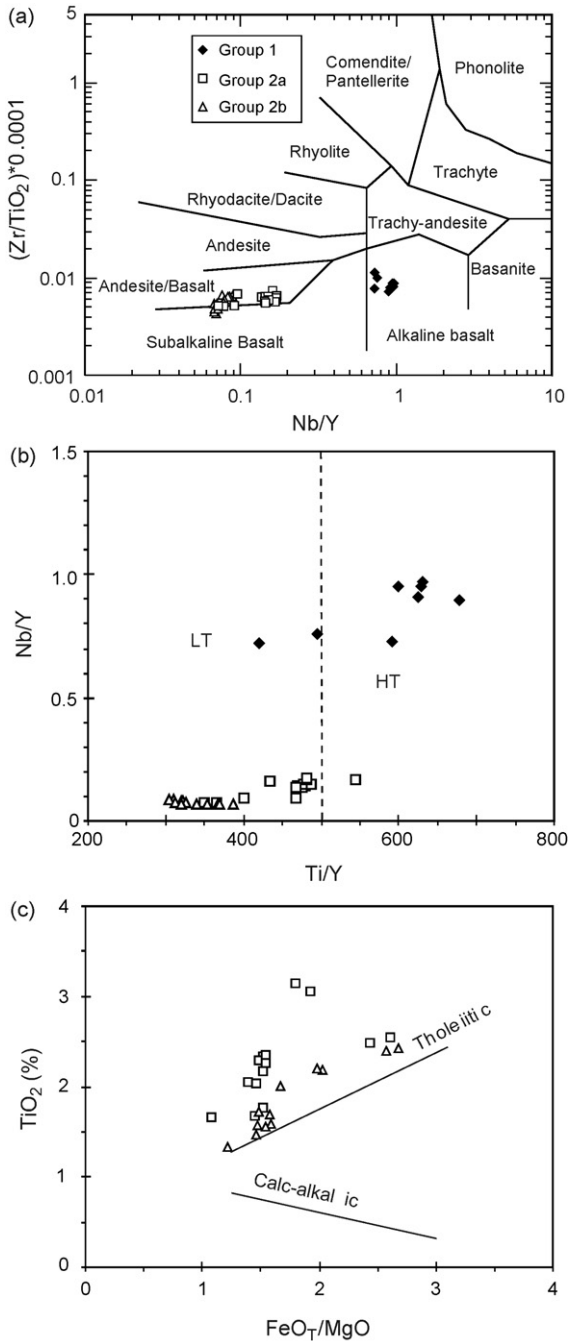


Fig. 8. Plots of (a) Nb/Y vs. Zr/TiO₂ (Winchester and Floyd, 1976), (b) Ti/Y vs. Nb/Y (Peate et al., 1992), (c) FeO_T/MgO vs. TiO₂ (Miyashiro, 1974) for classification of the mafic dykes. Symbols as in Fig. 6.

tholeiitic in composition and have nearly flat chondrite-normalized REE patterns, indicating that their residue phase was garnet-poor. Because garnet has a higher partition coefficient for Yb ($D=6.6$) than La ($D=0.0016$) (Johnson, 1998), minor residual garnet in the mantle source will significantly fractionate REE, leading to depletion in HREE. Fig. 14 indicates the presence of less than 1% residual garnet in the source region for the Group 2 rocks, and that the source was responsible for a spinel-stable field. Based on calculation of REE fractionation, the degree of partial melting for the Group 2 was about 7% (Fig. 14).

Thus, a residual spinel-stable field asthenospheric mantle source, which had undergone partial melting to form the melt for

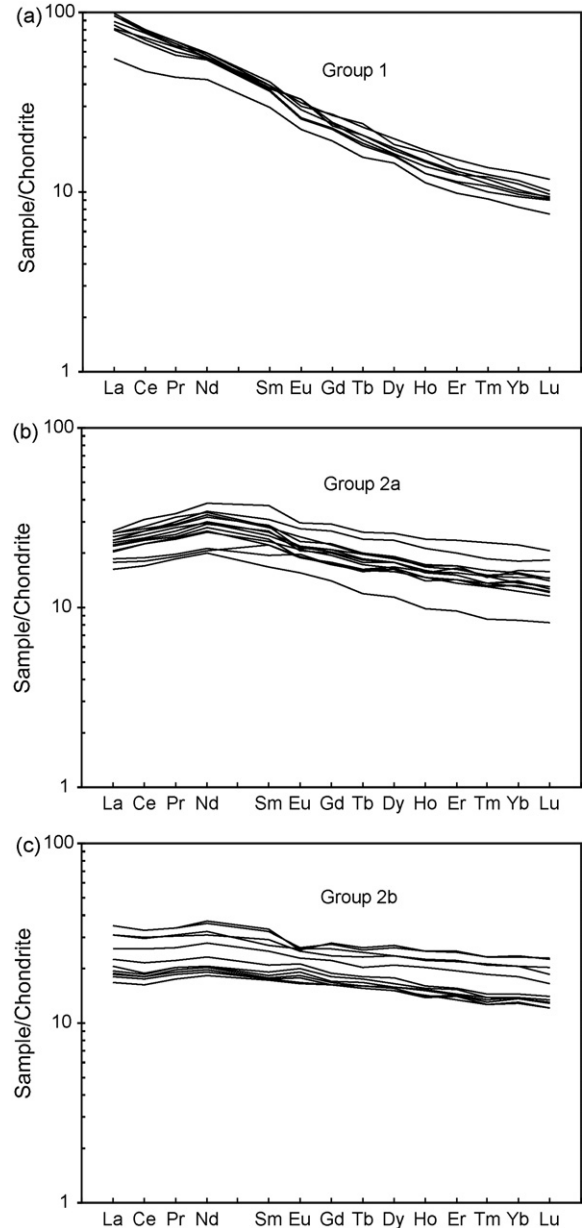


Fig. 9. Chondrite-normalized REE patterns of the mafic dykes in the Yanbian area. Normalizing values from Boynton (1984). (a) The Group 1, (b) the Group 2a, and (c) the Group 2b mafic dykes.

the Group 1, had experienced relatively higher degrees of partial melting to form the Group 2 rocks.

5.4. Tectonic significance

Extensive Neoproterozoic magmatic rocks in the western margin of the Yangtze Block range in age from 750 to 860 Ma, and their origin has been a long-standing issue of debate. They have been interpreted as the products either of a mantle plume (Z.X. Li et al., 1995, 1999) or of arc magmatism (Zhou et al., 2002a,b, 2006a,b). Our new data for the 790–760 Ma mantle-derived mafic dykes in the Yanbian area currently provide further constraints on the Neoproterozoic tectonic evolution in the western margin of the Yangtze Block.

The igneous assemblage in the Yanbian area, including mafic–ultramafic complexes, mafic dykes and metavolcanic rocks

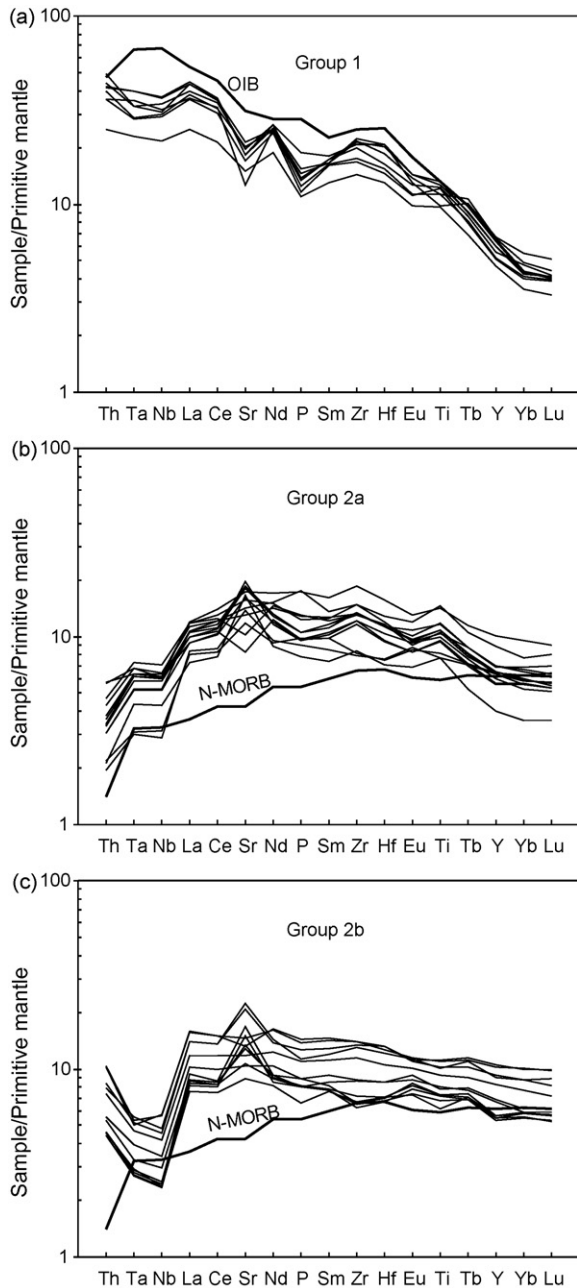


Fig. 10. Primitive mantle-normalized incompatible trace element spider diagram for the mafic dykes in the Yanbian area. Normalizing values from Sun and McDonough (1989). (a) The Group 1, (b) the Group 2a, and (c) the Group 2b mafic dykes.

of the Yanbian Group, previously was collectively termed the Proterozoic “Yanbian Ophiolite” (Geological Team 106 of SGBMR, 1975; Sun and Vuagnat, 1992; Sun, 1994). The mafic dyke swarms in this region show an obvious intrusive relationship with metavolcanic rocks of the Yanbian Group (Wang and Kan, 2001; Jiang et al., 2005). The present study indicates that the mafic dykes were emplaced at ca. 790–760 Ma, which are 30–60 Ma younger than the Gaojiacun and Lengshuiqing mafic–ultramafic complexes (Zhu et al., 2006, 2007). In addition, intrusive contacts were also observed between the Gaojiacun, Lengshuiqing complexes and metavolcanic rocks and schists of the Yanbian Group (Zhu et al., 2006, 2007). The geological relationships and U–Pb zircon ages imply that these magmatic rocks were not formed during a single magmatic event.

As a result, the mafic dykes and mafic–ultramafic complexes in the area cannot be part of an ophiolite.

Based on aforementioned discussions, the least-contaminated mafic dykes of the Group 1 exhibit characteristic patterns of incompatible trace element similar to those of OIB. In the discrimination diagrams of Ti–Zr–Y (Fig. 15a; Pearce and Cann, 1973), Zr/Y–Zr (Fig. 15b; Pearce and Norry, 1979), and La/10–Y/15–Nb/8 (Fig. 15c; Cabanis and Lecolle, 1989), the Group 1 rocks are plotted in the within-plate basalt field, indicating that the Group 1 might be derived from an OIB-like source in a continental rift environment. Furthermore, most of the less-contaminated rocks from the Group 2a are also plotted into the field of the within-plate basalt (Fig. 15a and b), suggesting the mafic dykes of the Group 2 could be also generated during an intra-continental rifting. In contrast, Group 2a rocks are plotted into the field of the continental back-arc tholeiites (Fig. 15c), most likely due to depletion in Nb and La caused by relatively higher degree melting of the spinel-stable mantle source. The Group 2b rocks exhibit some “arc-like” geochemical features (Fig. 15a and b), probably due to more crustal contamination than those of Group 2a. In addition, on the plot of Al_2 vs. TiO_2 in clinopyroxene of Loucks (1990), the clinopyroxenes of the Group 1 and Group 2a mafic dykes are strongly affinitive with rift-related, rather than arc-related, mafic–ultramafic cumulative rocks (Fig. 15d). Therefore, the mafic dykes in the Yanbian area were formed in a within-plate rift environment, rather than an arc environment.

The ages of the mafic dykes in the Yanbian area are similar to those of mafic dykes (ca. 780–760 Ma) in the Kangding and Shimian area (Z.X. Li et al., 2003; Lin et al., 2007), indicating that significant mafic magmatism occurred during 790–760 Ma along the western margin of the Yangtze Block. A tectono-magmatic model for production of the mafic dykes in this area is likely related to the mid-Neoproterozoic mantle plume, i.e., a plume arose at about 790–760 Ma from the deep mantle. The plume triggered low degree partial melting of the mantle OIB-like in the garnet-bearing field, followed by relatively higher degree melting of the refractory asthenospheric mantle source in the spinel-stable field. The low degrees of partial melting of OIB-like mantle source generated the parental magma of the Group 1 dykes with OIB geochemical affinity. The higher degree partial melting of the relatively refractory asthenospheric mantle source subsequently produced the parental magma of the Group 2 rocks. The progressive upwelling of asthenospheric mantle implies the existence of an anomalously hot mantle plume in the southwest China during the Neoproterozoic. As a result, this study supports the interpretation that the mafic dykes in the Yanbian area originated from a mantle plume-induced continental rift.

The 780 Ma mafic dyke swarm also occurred in western North American (Park et al., 1995), as well as widespread ca. 760–750 Ma mafic dykes in Western Australia and Seychelles. The 755 Ma Mundine Well dyke swarms (MDS) in northwestern Australia have been proposed to originate from a Neoproterozoic mantle plume (Ernst and Buchan, 2001; Z.X. Li et al., 2003; X.H. Li et al., 2006b). The Seychelles dolerites (Tucker et al., 2001; Ashwal et al., 2002), dated at 750 ± 3 Ma, have also been considered by most workers as being formed in a rift- or plume-related extensional tectonic setting (X.H. Li et al., 2006b). Such large-scale, transcontinental rifting and magmatism could be best explained by mantle plume or superplume activities beneath the super-continental Rodinia. This 790–760 Ma Neoproterozoic extensional event is responsible for the later stage of the Rodinia superplume cycle that started continental rifting within Rodinia at ca. 820–825 Ma. This proposal supports the idea that South China might have been located between Australia and Laurentia in the Rodinia supercontinent (Z.X. Li et al., 2003). In conclusion, the rift-related intra-continental setting of the mafic dykes

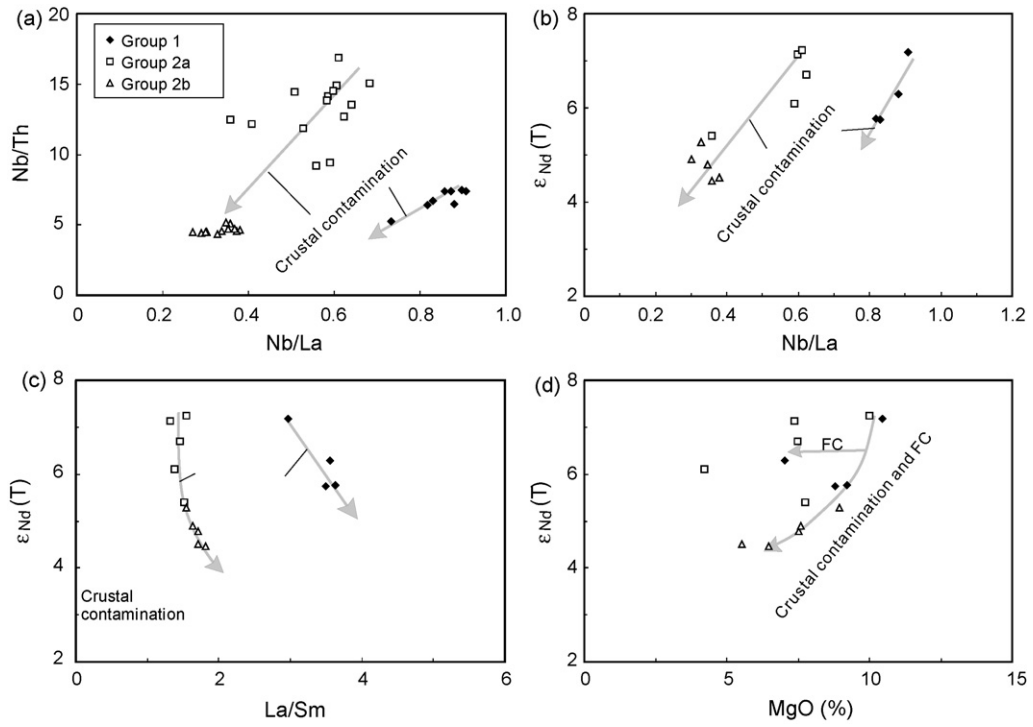


Fig. 11. Plots of (a) Nb/Th vs. Nb/La, (b) $\epsilon_{Nd}(T)$ vs. Nb/La (X.H. Li et al., 2006a), (c) $\epsilon_{Nd}(T)$ vs. La/Sm, and (d) $\epsilon_{Nd}(T)$ vs. MgO for the mafic dykes in the Yanbian area. Symbols as in Fig. 6.

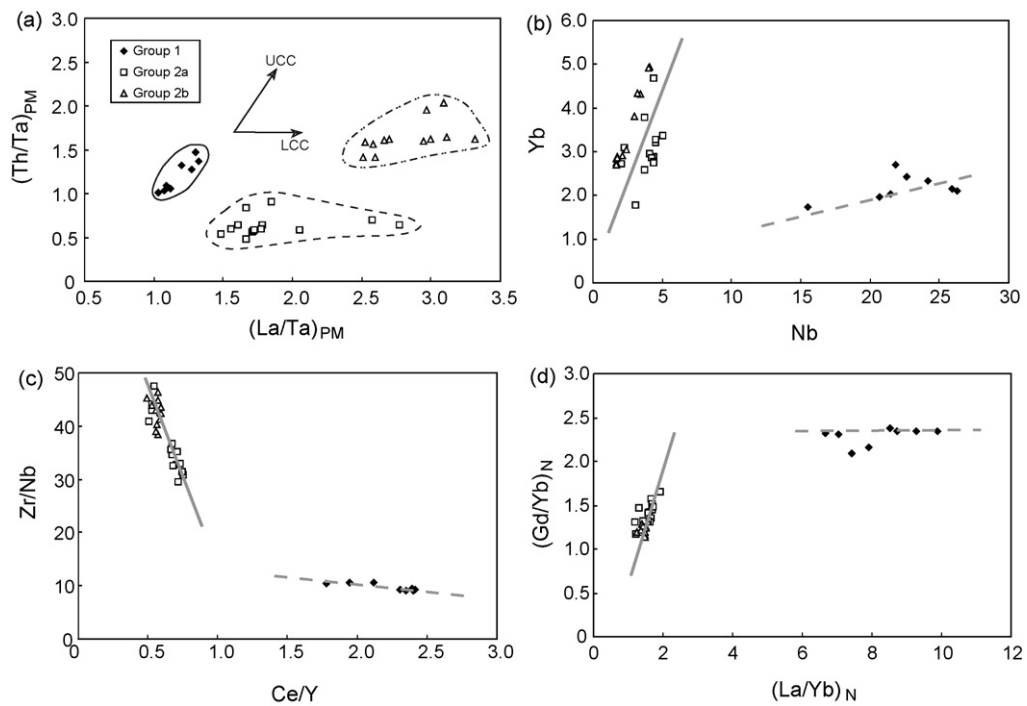


Fig. 12. Plots of (a) $(Th/Ta)_{PM}$ vs. $(La/Ta)_{PM}$ (Ingle et al., 2002), (b) Yb vs. Nb, (c) Zr/Nb vs. Ce/Y, and (d) $(Gd/Yb)_N$ vs. $(La/Yb)_N$ for the mafic dykes in the Yanbian area. Symbols as in Fig. 6.

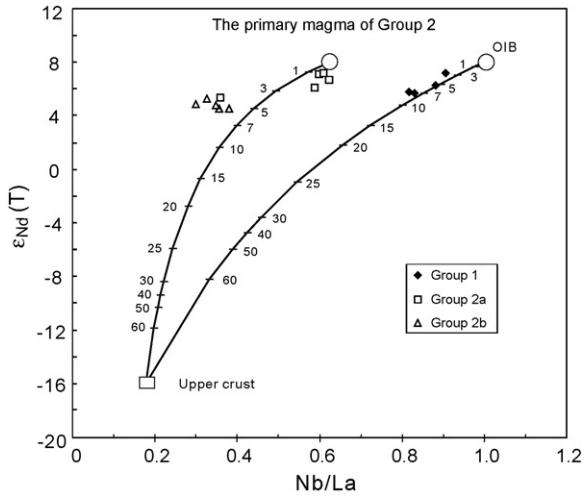


Fig. 13. Plot of $\epsilon_{Nd}(T)$ vs. Nb/La for the mafic dykes showing the effects of crustal contamination. Numbers labeled on the binary mixing curve represent the percentages of crust added to the melt. The contaminant crustal components (La = 64.5 ppm, Nd = 38.1 ppm, Nb = 11.4 ppm, and $\epsilon_{Nd}(790 \text{ Ma}) = -16$) are the average of the metasedimentary rocks from the Huili Group in the Yangtze Block (our unpublished data). The primary magmas for OIB are assumed having Nb/La = 1, La = 22.4 ppm, Nd = 27.4 ppm, and $\epsilon_{Nd}(T) = +8$ from the least-contaminated alkaline basalt in the Suxiong volcanics (X.H. Li et al., 2002a). The primary magmas of Group 2 are assumed having Nb/La = 0.62, La = 4.8 ppm, Nd = 11.8 ppm, and $\epsilon_{Nd} = +8$, similar to four least-contaminated mafic dykes having N-MORB-like trace element features in the Kangding–Shimian area (Lin et al., 2007).

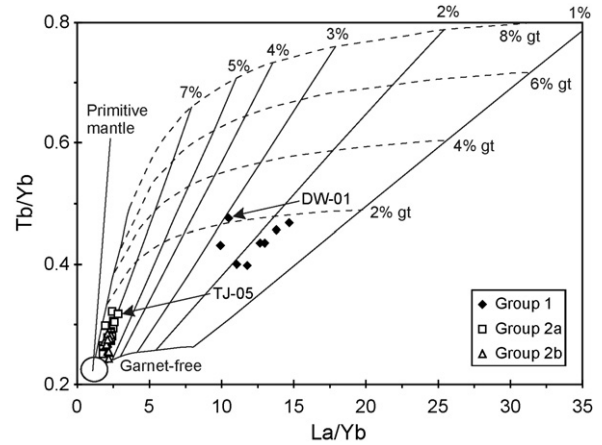


Fig. 14. Plot of La/Yb and Tb/Yb for the mafic dykes in the Yanbian area. The model assumes a garnet mode in the source varying from 0 to 8% (subhorizontal lines) (with olivine at 55%, orthopyroxene at 25%, and clinopyroxene at >12% entering the melt phase in the proportions 20:20:40:20%, respectively). Melt increments are shown as subvertical lines in 1% intervals between 1 and 7%. The melting curves are from George and Rogers (2002). Partition coefficients employed are from the compilation of McKenzie and O'Nions (1991). Symbols as in Fig. 6.

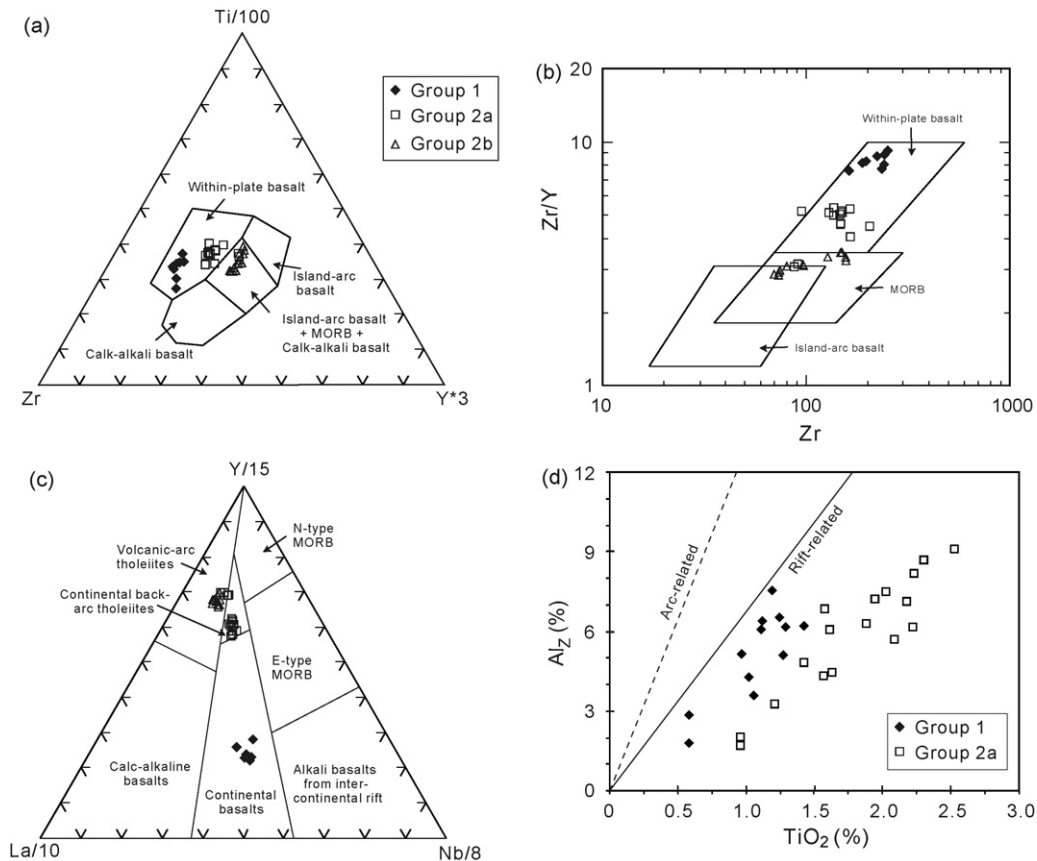


Fig. 15. Discrimination diagrams of (a) Ti–Zr–Y (Pearce and Cann, 1973), (b) Zr/Y–Zr (Pearce and Norry, 1979), (c) La/10–Y/15–Nb/8 (Cabanis and Lecolle, 1989), and (d) Al_z (percentage of tetrahedral sites occupied by Al) vs. TiO₂ in clinopyroxenes (Loucks, 1990) for the mafic dykes in the Yanbian area. Symbols as in Fig. 6.

in the Yanbian area indicates the manifestation of a Neoproterozoic Rodinia super-continental breakup.

Acknowledgements

We appreciate the assistances of G.F. Zhou, W.Q. Zheng, and S.R. Liu for electron microprobe analysis, D.Y. Liu, B. Song, Y.S. Wan, Z.Q. Yang, Y.R. Shi and H. Tao in SHRIMP dating, C.X. Feng in major element analyses by XRF, X.L. Tu, Y. Liu, Y.P. Wang, J. Hu, and Y.R. Cai for trace element analyses by ICP-MS, Z.Y. Chu and C.F. Li for Nd isotope

analyses by TIMS, and to X.C. Wang in simulation calculation. The paper has benefited from constructive comments of Z.X. Li, W.X. Li, H.F. Tang, C. Xu, two anonymous reviewers and the associate editor P.A. Cawood. This work is jointly supported by the “CAS Hundred Talents” Foundation of the Chinese Academy of Sciences, 973 Program (2007CB411401) and NSFC (Grants 40673031, 40421303, and 40673030).

Appendix A. Clinopyroxene compositions for the mafic dykes in the Yanbian area

Sample	HT-01	HT-01	HT-01	DW-01	DW-01	DW-01	HT-05	HT-05	HT-05	04HS-09	04HS-09	04HS-09	XF-04	XF-04	XF-04
SiO ₂	50.51	50.98	50.71	51.74	52.90	53.93	50.69	50.43	49.84	52.04	49.14	49.73	50.61	49.50	51.09
TiO ₂	1.10	0.96	1.26	1.04	0.58	0.58	1.42	1.28	1.23	1.02	1.17	1.10	1.62	1.86	1.20
Al ₂ O ₃	4.15	4.07	3.70	3.56	1.90	1.86	4.65	4.44	4.46	3.31	4.68	4.04	2.63	3.90	2.19
Cr ₂ O ₃	0.50	0.43	0.04	0.43	0.31	0.32	0.51	0.55	0.32	0.04	0.17	0.47	0.01	0.00	0.00
MgO	15.60	15.22	15.17	15.92	18.37	18.03	15.01	15.74	15.14	15.81	15.03	15.46	13.77	13.50	13.75
CaO	20.37	20.24	19.41	18.98	18.44	18.75	20.08	19.44	19.67	19.87	20.31	20.40	19.26	19.63	18.65
MnO	0.15	0.17	0.18	0.18	0.21	0.15	0.18	0.16	0.19	0.18	0.19	0.17	0.32	0.28	0.44
FeO	6.58	6.67	8.05	5.78	6.67	6.29	6.84	6.53	7.55	7.88	7.71	6.49	10.72	9.81	11.39
NiO	0.04	0.01	0.06	0.02	0.05	0.03	0.01	0.02	0.02	0.03	0.02	0.02	0.02	0.03	0.00
ZnO	0.04	0.00	0.00	0.00	0.02	0.00	0.05	0.00	0.01	0.02	0.05	0.00	0.02	0.02	0.06
Na ₂ O	0.26	0.32	0.33	0.37	0.24	0.22	0.29	0.34	0.31	0.24	0.34	0.36	0.43	0.42	0.38
K ₂ O	0.01	0.00	0.00	0.00	0.00	0.02	0.01	0.00	0.01	0.00	0.00	0.00	0.00	0.00	0.01
Total	99.30	99.08	98.90	98.02	99.70	100.18	99.74	98.91	98.74	100.45	98.82	98.23	99.40	98.95	99.16
Si	1.88	1.90	1.90	1.93	1.94	1.96	1.88	1.88	1.87	1.91	1.85	1.87	1.91	1.87	1.94
Ti	0.03	0.03	0.04	0.03	0.02	0.02	0.04	0.04	0.03	0.03	0.03	0.03	0.05	0.05	0.03
Al	0.18	0.18	0.16	0.16	0.08	0.08	0.20	0.19	0.20	0.14	0.21	0.18	0.12	0.17	0.10
Cr	0.01	0.01	0.00	0.01	0.01	0.01	0.01	0.02	0.01	0.00	0.01	0.01	0.00	0.00	0.00
Fe ³⁺	0.00	0.00	0.00	0.00	0.00	0.00	0.00	0.00	0.00	0.00	0.00	0.00	0.00	0.00	0.00
Mg	0.86	0.84	0.85	0.88	1.01	0.98	0.83	0.87	0.85	0.87	0.84	0.87	0.78	0.76	0.78
Ca	0.80	0.80	0.77	0.75	0.72	0.72	0.79	0.77	0.78	0.77	0.81	0.81	0.77	0.79	0.75
Mn	0.00	0.01	0.01	0.01	0.01	0.00	0.01	0.00	0.01	0.01	0.01	0.01	0.01	0.01	0.01
Fe ²⁺	0.20	0.21	0.25	0.18	0.20	0.19	0.21	0.20	0.24	0.24	0.24	0.20	0.34	0.31	0.36
Ni	0.00	0.00	0.00	0.00	0.00	0.00	0.00	0.00	0.00	0.00	0.00	0.00	0.00	0.00	0.00
Na	0.02	0.02	0.02	0.03	0.02	0.02	0.02	0.02	0.02	0.02	0.03	0.03	0.03	0.03	0.03
En	46.24	45.67	45.34	48.80	52.18	51.71	45.35	47.42	45.41	46.05	44.50	46.05	41.17	41.00	41.20
Fs	10.94	11.23	13.50	9.93	10.64	10.13	11.59	11.04	12.70	12.88	12.81	10.84	17.97	16.71	19.15
Wo	42.83	43.10	41.16	41.27	37.19	38.16	43.06	41.55	41.88	41.08	42.69	43.11	40.86	42.29	39.66
Sample	XF-04	XF-04	TJ-04	TJ-04	TJ-04	TJ-04	TJ-07	TJ-07	TJ-07	TJ-07	TJ-07	HL-03	HL-03	HL-03	HL-03
SiO ₂	50.15	49.44	50.22	49.84	52.60	47.77	50.19	48.28	46.81	48.68	50.51	51.23	49.44	48.82	
TiO ₂	1.60	1.59	1.55	2.24	0.97	2.19	2.09	2.53	2.24	2.16	1.43	0.96	1.95	2.01	
Al ₂ O ₃	3.63	3.91	2.84	3.27	1.42	4.87	3.75	5.42	4.20	4.41	3.14	1.40	4.53	4.37	
Cr ₂ O ₃	0.01	0.00	0.07	0.00	0.00	0.07	0.01	0.07	0.01	0.07	0.01	0.00	0.06	0.04	
MgO	14.15	13.68	12.22	12.53	14.55	11.40	12.48	11.98	12.11	11.70	12.88	10.37	12.93	13.07	
CaO	19.97	18.23	20.47	20.45	18.09	20.84	19.96	21.35	20.13	20.40	20.69	19.40	20.94	20.54	
MnO	0.37	0.31	0.33	0.29	0.47	0.24	0.34	0.24	0.28	0.24	0.35	0.66	0.24	0.23	
FeO	11.14	11.24	10.71	11.48	12.52	10.49	10.94	9.85	11.13	10.91	10.47	15.54	9.43	9.60	
NiO	0.01	0.00	0.02	0.00	0.01	0.02	0.01	0.00	0.04	0.00	0.01	0.03	0.00	0.03	
ZnO	0.00	0.00	0.06	0.00	0.03	0.10	0.01	0.08	0.09	0.00	0.00	0.10	0.03	0.00	
Na ₂ O	0.54	0.38	0.40	0.40	0.18	0.45	0.36	0.40	0.40	0.44	0.35	0.35	0.42	0.42	
K ₂ O	0.00	0.01	0.00	0.00	0.00	0.01	0.00	0.00	0.00	0.00	0.00	0.00	0.00	0.01	
Total	101.55	98.78	98.90	100.49	100.84	98.46	100.13	100.19	97.43	98.99	99.82	100.03	99.98	99.14	
Si	1.86	1.88	1.91	1.88	1.96	1.84	1.89	1.82	1.83	1.86	1.90	1.97	1.86	1.85	
Ti	0.04	0.05	0.04	0.06	0.03	0.06	0.06	0.07	0.07	0.06	0.04	0.03	0.05	0.06	
Al	0.16	0.17	0.13	0.15	0.06	0.22	0.17	0.24	0.19	0.20	0.14	0.06	0.20	0.20	
Cr	0.00	0.00	0.00	0.00	0.00	0.00	0.00	0.00	0.00	0.00	0.00	0.00	0.00	0.00	
Fe ³⁺	0.00	0.00	0.00	0.00	0.00	0.00	0.00	0.00	0.00	0.00	0.00	0.00	0.00	0.00	
Mg	0.78	0.77	0.69	0.70	0.81	0.65	0.70	0.67	0.70	0.67	0.72	0.59	0.72	0.74	
Ca	0.78	0.73	0.83	0.81	0.71	0.85	0.79	0.85	0.83	0.82	0.82	0.79	0.83	0.82	
Mn	0.01	0.01	0.01	0.01	0.01	0.01	0.01	0.01	0.01	0.01	0.01	0.02	0.01	0.01	
Fe ²⁺	0.35	0.36	0.34	0.36	0.39	0.34	0.34	0.31	0.36	0.35	0.33	0.50	0.30	0.30	
Ni	0.00	0.00	0.00	0.00	0.00	0.00	0.00	0.00	0.00	0.00	0.00	0.00	0.00	0.00	
Na	0.04	0.03	0.03	0.03	0.01	0.03	0.03	0.03	0.03	0.03	0.03	0.03	0.03	0.03	
En	40.93	41.55	37.31	37.42	42.29	35.56	38.07	36.68	37.11	36.23	38.53	31.56	39.09	39.58	
Fs	18.08	19.15	18.34	19.23	20.41	18.35	18.73	16.91	19.13	18.95	17.56	26.54	15.99	16.30	
Wo	40.99	39.29	44.34	43.35	37.30	46.09	43.20	46.41	43.75	44.83	43.91	41.90	44.92	44.12	

References

- Barth, M.G., McDonough, W.F., Rudnick, R.L., 2000. Tracking the budget of Nb and Ta in the continental crust. *Chem. Geol.* 165, 197–213.
- Ashwal, L.D., Demaiffe, D., Torsvik, T.H., 2002. Petrogenesis of Neoproterozoic granitoids and related rocks from the Seychelles: the case for an Andean-type arc origin. *J. Petrol.* 43, 45–83.
- Black, L.P., Kamo, S.L., Allen, C.M., Aleinikov, J.N., Davis, D.W., Korsch, R.J., Foudoulis, C., 2003. TEMORA 1: a new zircon standard for Phanerozoic U–Pb geochronology. *Chem. Geol.* 200, 155–170.
- Boynton, W.V., 1984. Geochemistry of the rare earth elements: meteorite studies. In: Henderson, P. (Ed.), *Rare Earth Element Geochemistry*. Elsevier, pp. 63–114.
- Cabanis, B., Lecolle, M., 1989. Le diagramme La/10–Y/15–Nb/8: un outil pour la discrimination des series volcaniques et la mise en evidence des processus de melange et/ou de contamination crutale. *C.R. Acad. Sci. Ser. II* 309, 2023–2029.
- Compston, W., Williams, I.S., Kirschvink, J.L., Zhang, Z., Ma, G., 1992. Zircon U–Pb ages for the early Cambrian time-scale. *J. Geol. Soc. Lond.* 149, 171–184.
- Cong, B.L., 1988. Formation and Evolution of Panxi paleo-rift. Science Press, Beijing, pp. 267–314 (in Chinese).
- Cullers, R.L., Graf, J.L., 1984. Rare earth elements in igneous rocks of the continental crust: predominantly basic and ultrabasic rocks. In: Henderson, P. (Ed.), *Rare Earth Element Geochemistry*. Elsevier, Amsterdam, pp. 237–274.
- Deniel, C., 1998. Geochemical and isotopic (Sr, Nd, Pb) evidence for plume–lithosphere interactions in the genesis of Grande Comore magmas (Indian Ocean). *Chem. Geol.* 144, 281–303.
- Ernst, R.E., Buchan, K.L., 2001. Large mafic magmatic events through time and links to mantle–plume heads. In: Ernst, R.E., Buchan, K.L. (Eds.), *Mantle Plumes: Their Identification Through Time*. Geological Society of America, Special Paper 352, pp. 483–575.
- Ewart, A., Milner, S.C., Armstrong, R.A., Duncan, A.R., 1998. Etendeka volcanism of the Goboboseb Mountains and Messum igneous complex, Namibia. Part I. Geochemical evidence of early Cretaceous Tristan Plume melts and the role of crustal contamination in the Parana–Etendeka CFB. *J. Petrol.* 39, 191–225.
- Garland, F., Turne, S., Hawkesworth, C., 1996. Shifts in the source of the Parana basalts through time. *Lithos* 37, 223–243.
- Geological Team 106 of Sichuan Bureau of Geology and Mineral Resource (SBGMR), 1975. Pre-Sinian geologic features of middle section of Kangdian axis and its relationship to relate tectonics. *Sci. Geol. Sin.* 2, 107–113 (in Chinese).
- George, R.M., Rogers, N.W., 2002. Plume dynamics beneath the African plate inferred from the geochemistry of the Tertiary basalts of southern Ethiopia. *Contrib. Mineral. Petrol.* 144, 286–304.
- Gibson, S.A., Kirkpatrick, R.J., Emmerman, R., Schmincke, P.H., Pritchard, G., Okay, P.J., Horpe, R.S., Marriner, G.F., 1982. The trace element composition of the lavas and dykes from a 3 km vertical section through a lava pile of Eastern Iceland. *J. Geophys. Res.* 87, 6532–6546.
- Greentree, M.R., Li, Z.X., Li, X.H., Wu, H.C., 2006. Late Mesoproterozoic to earliest Neoproterozoic basin record of the Sibao orogenesis in western South China and relationship to the assembly of Rodinia. *Precambrian Res.* 151, 79–100.
- Hirschmann, M.M., Ghiorso, M.S., Wasylenski, L.E., Asimow, P.D., Stolper, E.M., 1998. Calculation of peridotite partial melting from thermodynamic models of minerals and melts. I. Method and composition to experiments. *J. Petrol.* 39, 1091–1115.
- Ingle, S., Weis, D., Scoates, J.S., Frey, F.A., 2002. Relationship between the early Kerguelen plume and continental flood basalts of the paleo-eastern Gondwanan margins. *Earth Planet. Sci. Lett.* 197, 35–50.
- Jiang, Y.B., Zhang, S.H., Wu, H.C., Han, Y.G., 2005. Study on stratum characteristic and geotectonic feature on the Yanbian Group. *J. East China Inst. Technol.* 28, 347–353 (in Chinese).
- Johnson, K.T.M., 1998. Experimental determination of partition coefficients for rare earth and high-field-strength elements between clinopyroxene, garnet, and basaltic melt at high pressures. *Contrib. Mineral. Petrol.* 133, 60–68.
- Li, X.H., Li, Z.X., Zhou, H., Liu, Y., Liang, X.Y., Li, W.X., 2003a. SHRIMP U–Pb zircon age, geochemistry and Nd isotope of the Guandaoshan pluton in SW Sichuan: petrogenesis and tectonic significance. *Sci. China (Ser. D)* 46 (Suppl.), 73–83.
- Li, X.H., Li, Z.X., Ge, W., Zhou, H.W., Li, W.X., Liu, Y., Wingate, M.T.T., 2003b. Neoproterozoic granitoids in South China: crustal melting above a mantle plume at ca. 825 Ma? *Precambrian Res.* 122, 45–83.
- Li, X.H., Li, Z.X., Sinclair, J.A., Li, W.H., Carter, G., 2007a. Understanding dual geochemical characters in a geological context for the Gaojiacun intrusion: response to Munteanu and Yao's discussion [Precambrian Res. 154 (2007), this issue]. *Precambrian Res.* 155, 328–332.
- Li, X.H., Li, Z.X., Sinclair, J.A., Li, W.H., Carter, G., 2007b. Reply to the comment by Zhou et al. on: "Revisiting the "Yanbian Terrane": implications for Neoproterozoic tectonic evolution of the western Yangtze Block, South China" [Precambrian Res. 151 (2006) 14–30] [Precambrian Res. 154 (2007), this issue]. *Precambrian Res.* 155, 318–323.
- Li, X.H., Li, Z.X., Sinclair, J.A., Li, W.X., Carter, G., 2006a. Revisiting the "Yanbian Terrane": implications for Neoproterozoic tectonic evolution of the western Yangtze Block, South China. *Precambrian Res.* 151, 14–30.
- Li, X.H., Li, Z.X., Wingate, M.T.D., Chung, S.L., Liu, Y., Lin, G.C., Li, W.X., 2006b. Geochemistry of the 755 Ma Mundine Well dyke swarm, northwestern Australia: part of a Neoproterozoic mantle superplume beneath Rodinia? *Precambrian Res.* 146, 1–15.
- Li, X.H., Li, Z.X., Zhou, H., Liu, Y., Kinny, P.D., 2002a. U–Pb zircon geochronology, geochemistry and Nd isotopic study of Neoproterozoic bimodal volcanic rocks in the Kangding Rift of South China: implications for the initial rifting of Rodinia. *Precambrian Res.* 113, 135–155.
- Li, X.H., Li, Z.X., Zhou, H., Liu, Y., Liang, X.H., 2002b. U–Pb zircon geochronological, geochemical and Nd isotopic study of Neoproterozoic basaltic magmatism in western Sichuan: petrogenesis and geodynamic implications. *Earth Sci. Front.* 9, 329–338 (in Chinese).
- Li, X.H., Sun, M., Wei, G.J., Liu, Y., Lee, C.Y., Malpas, J., 2000. Geochemical and Sm–Nd isotopic study of amphibolites in the Cathaysia Block, southeastern China: evidence for an extremely depleted mantle in the Paleoproterozoic. *Precambrian Res.* 102, 251–262.
- Li, Z.X., Li, X.H., Kinny, P.D., Wang, J., 1999. The breakup of Rodinia: did it start with a mantle plume beneath South China? *Earth Planet. Sci. Lett.* 173, 171–181.
- Li, Z.X., Li, X.H., Kinny, P.D., Wang, J., Zhang, S., Zhou, H., 2003. Geochronology of Neoproterozoic syn-rift magmatism in the Yangtze Craton, South China and correlations with other continents: evidence for a mantle superplume that broke up Rodinia. *Precambrian Res.* 122, 85–109.
- Li, Z.X., Li, X.H., Zhou, H., Kinny, P.D., 2002. Grenvillian continental collision in South China: new SHRIMP U–Pb zircon results and implications for the configuration of Rodinia. *Geology* 30, 163–166.
- Li, Z.X., Zhang, L., Powell, C.M., 1995. South China in Rodinia: part of the missing link between Australia–East Antarctica and Laurentia? *Geology* 23, 407–410.
- Lightfoot, P.C., Hawkesworth, C.J., Hergt, J., Naldrett, A.J., Gorbachev, N.S., Fedorenko, V.A., Doherty, W., 1993. Remobilisation of the continental lithosphere by a mantle plume: major-, trace-element, and Sr-, Nd-, and Pb-isotope evidence from picritic and tholeiitic lavas of the Noril'sk District, Siberian Trap, Russia. *Contrib. Mineral. Petrol.* 114, 171–188.
- Lin, G.C., Li, X.H., Li, W.X., 2007. SHRIMP U–Pb zircon age, geochemistry and Nd–Hf isotope of Neoproterozoic mafic dyke swarms in western Sichuan: petrogenesis and tectonic significance. *Sci. China (Ser. D)* 50, 1–16.
- Loucks, R.R., 1990. Discrimination of ophiolitic from nonophiolitic ultramafic–mafic allochthons in orogenic belts by the Al/Ti ratio in clinopyroxene. *Geology* 18, 346–349.
- Lugmair, G.W., Hart, K., 1978. Lunar initial $^{143}\text{Nd}/^{144}\text{Nd}$: differential evolution of the lunar crust and mantle. *Earth Planet. Sci. Lett.* 39, 349–357.
- McKenzie, D.P., O'Nions, R.K., 1991. Partial melt distributions from inversion of rare earth element concentrations. *J. Petrol.* 32, 1021–1091.
- Miyashiro, A., 1974. Volcanic rock series in island arc and active continental margins. *Am. J. Sci.* 274, 321–355.
- Munteanu, M., Yao, Y., 2007. The Gaojiacun intrusion: rift- or subduction-related? Comment on "Revisiting the "Yanbian Terrane": implications for Neoproterozoic tectonic evolution of the western Yangtze Block, South China" by Li et al. (2006) [Precambrian Res. 151 (2006) 14–30]. *Precambrian Res.* 155, 324–327.
- Paces, J.B., Bell, K., 1989. Non-depleted sub-continental mantle beneath the Superior Province of the Canadian Shield: Nd–Sr isotopic and trace element evidence from mid-continent rift basalts. *Geochim. Cosmochim. Acta* 53, 2023–2035.
- Park, J.K., Buchan, K.L., Harlan, S.S., 1995. A proposed giant radiating dyke swarm fragmented by the separation of Laurentia and Australia based on paleomagnetism of ca. 780 Ma mafic intrusions in western North America. *Earth Planet. Sci. Lett.* 132, 129–139.
- Pearce, J.A., Cann, J.R., 1973. Tectonic setting of basic volcanic rocks determined using trace element analysis. *Earth Planet. Sci. Lett.* 19, 290–300.
- Pearce, J.A., Norry, M.J., 1979. Petrogenetic implications of Ti, Zr, Y, and Nb variations in volcanic rocks. *Contrib. Mineral. Petrol.* 69, 33–47.
- Peate, D.W., Hawkesworth, C.J., Mantovani, M.S.M., 1992. Chemical stratigraphy of the Parana lavas South America: classification of magma-types and their spatial distribution. *Bull. Volcanol.* 55, 119–139.
- Pik, R., Deniel, C., Coulon, C., Yirgu, G., Hofmann, C., Ayalew, D., 1998. The north-western Ethiopian plateau flood basalts: classification and spatial distribution of magma types. *J. Volcanol. Geotherm. Res.* 81, 91–111.
- Pik, R., Deniel, C., Coulon, C., Yirgu, G., Marty, B., 1999. Isotopic and trace element signatures of Ethiopian flood basalts: evidence for plume–lithosphere interaction. *Geochim. Cosmochim. Acta* 63, 2263–2279.
- Roeder, P.L., Emslie, R.F., 1970. Olivine–liquid equilibrium. *Contrib. Mineral. Petrol.* 29, 275–289.
- Rudnick, R.L., Fountain, D.M., 1995. Nature and composition of the continental crust: a lower crustal perspective. *Rev. Geophys.* 33, 267–309.
- Shen, W.Z., Gao, J.F., Xu, S.J., Tan, G.Q., Yang, Z.S., Yang, Q.W., 2003. Format on age and geochemical characteristics of the Lengshuiqing body, Yanbian, Sichuan province. *Acta Petrol. Sin.* 19, 27–37 (in Chinese).
- Shen, W.Z., Gao, J.F., Xu, S.J., Zhou, G.Q., 2002. Geochemical characteristics and genesis of the Qiaotou basic complex, Luding County, western Yangtze Block. *Geol. J. China Univ.* 8, 380–389 (in Chinese).
- Sichuan Bureau of Geology (SBG), 1972. A report of regional geological survey in Yanbian area of the People's Republic of China (the scale of 1:200000) (in Chinese).
- Sichuan Bureau of Geology and Mineral Resource (SBGMR), 1991. Regional Geology of Sichuan Province. Geol. Publ. House, Beijing, 730 pp. (in Chinese with English abstract).
- Sinclair, J.A., 2001. A re-examination of the "Yanbian Ophiolite Suite": evidence for western extension of the Mesoproterozoic Sibao Oregon in South China. *Geol. Soc. Aus.* 65, 99–100 (Abstract).
- Song, B., Zhang, Y.H., Wan, Y.S., Jian, P., 2002. Mount making and procedure of the SHRIMP dating. *Geol. Rev.* 48, 26–30 (Suppl., in Chinese).
- Stewart, K., Rogers, N., 1996. Mantle plume and lithosphere contributions to basalts from southern Ethiopia. *Earth Planet. Sci. Lett.* 139, 195–211.

- Su, L., Song, S.G., Song, B., Zhou, D.W., Hao, J.R., 2004. SHRIMP zircon U–Pb ages of garnet pyroxenite and Fushui gabbroic complex in Songshugou region and constraints on tectonic evolution of Qinling Orogenic Belt. *Chin. Sci. Bull.* 40, 1307–1310.
- Sun, C.M., 1994. Genetic mineralogy of pyroxenes from the Yanbain Proterozoic ophiolite (Sichuan, China), and its geotectonic implications. *Min. Rocks* 14, 1–15 (in Chinese).
- Sun, C.M., Vuagnat, M., 1992. Proterozoic ophiolites from Yanbian and Shimian (Sichuan province, China): petrography, geochemistry, petrogenesis, and geotectonic environment. *Schweiz Mineral. Petrogr. Mitt.* 72, 389–413.
- Sun, S.-S., McDonough, W.F., 1989. Chemical and isotopic systematics of oceanic basalts: implications for mantle composition and processes. In: Saunders, A.D., Norry, M.J. (Eds.), *Magmatism in the Ocean Basins*. Geol. Soc. Spec. Publ. no. 42, pp. 313–345.
- Sun, S.-S., Sherraton, J.W., 1996. Geochemical and isotopic evolution. In: Glikson, A.Y., et al. (Eds.), *Geology of the Western Musgrave Block, Central Australia*, with Particular Reference to the Mafic–Ultramafic Giles Complex. *Aust. Geol. Surv. Org. (AGSO) Bull.* 239, pp. 135–143.
- Thirlwall, M.F., Upton, B.G.J., Jenkins, C., 1994. Interaction between continental lithosphere and the Iceland plume–Sr–Nd–Pb isotope geochemistry of Tertiary basalts, NE Greenland. *J. Petrol.* 35, 839–879.
- Tucker, R.D., Ashwal, L.D., Torsvik, T.H., 2001. U–Pb geochronology of Seychelles granulites: a Neoproterozoic continental arc fragment. *Earth Planet. Sci. Lett.* 187, 27–38.
- Wang, J., Li, Z.X., 2003. History of Neoproterozoic rift basins in South China: implications for Rodinia break-up. *Precambrian Res.* 122, 141–158.
- Wang, K.M., Kan, Z.Z., 2001. Geological response to formation of the Rodinia supercontinent in western margin of the Yangtze platform. *Geol. Mineral. Resour. South China* (4), 22–27 (in Chinese).
- Wang, K., Plank, T., Walker, J.D., Smith, E.I., 2002. A mantle melting profile across the Basin and Range, SW USA. *J. Geophys. Res., Solid Earth* 107 (B1), 2017, doi:10.1029/2001JB000209.
- Wang, X.C., Li, X.H., Li, W.X., Li, Z.X., 2007. Ca. 825 Ma komatiitic basalts in South China: first evidence for >1500 °C mantle melts by a Rodinian mantle plume. *Geology* 35, 1103–1106.
- Wang, Y.J., Fan, W.M., Zhang, Y.H., Guo, F., Zhang, H.F., Peng, T.P., 2004. Geochemical, $^{40}\text{Ar}/^{39}\text{Ar}$ geochronological and Sr–Nd isotopic constraints on the origin of Paleoproterozoic mafic dikes from the southern Taihang Mountains and implications for the ca. 1800 Ma event of the North China Craton. *Precambrian Res.* 135, 55–77.
- Winchester, J.A., Floyd, P.A., 1976. Geochemical magma type discrimination: application to altered and metamorphosed igneous rocks. *Earth Planet. Sci. Lett.* 45, 326–336.
- Wingate, M.T.D., Campbell, I.H., Compston, W., Gibson, G.M., 1998. Ion microprobe U–Pb ages for Neoproterozoic basaltic magmatism in south-central Australia and implications for the breakup of Rodinia. *Precambrian Res.* 87, 135–159.
- Wingate, M.T.D., Giddings, J.W., 2000. Age and palaeomagmatism of the Mundine Well dyke swarm, Western Australia: implications for an Australia–Laurentia at 755. *Precambrian Res.* 100, 335–357.
- Wood, B., Blundy, J., 1997. A predictive model for rare earth element partitioning between clinopyroxene and anhydrous silicate melt. *Contrib. Mineral. Petrol.* 129, 166–181.
- Wood, D.A., Joron, J.L., Treuil, M., 1979. A re-appraisal of the use of trace elements to classify and discriminate between magma series erupted in different tectonic settings. *Earth Planet. Sci. Lett.* 45, 326–336.
- Xu, Y.G., Chung, S.L., Jahn, B.M., Wu, G.Y., 2001. Petrologic and geochemical constraints on the petrogenesis of Permian-Triassic Emeishan flood basalts in southwestern China. *Lithos* 58, 145–168.
- Zhang, H.F., Sun, M., Lu, F.X., Zhou, X.H., Zhou, M.F., Liu, Y.S., Zhang, G.H., 2001. Moderately depleted lithospheric mantle underneath the Yangtze Block: evidence from a garnet lherzolite xenolith in the Dahongshan kimberlite. *Geochem. J.* 35, 315–331.
- Zhao, J.H., Zhou, M.F., 2007. Geochemistry of Neoproterozoic mafic intrusions in the Panzhihua district (Sichuan Province, SW China): implications for subduction-related metasomatism in the upper mantle. *Precambrian Res.* 152, 27–47.
- Zhao, J.X., McCulloch, M.T., Jorsch, R.J., 1994. Characterisation of a plume-related ~800 Ma magmatic event and its implications for basin formation in central-southern Australia. *Earth Planet. Sci. Lett.* 121, 349–367.
- Zhao, J.X., McCulloch, M.T., 1993. Sm–Nd mineral isochron ages of late Proterozoic dyke swarms in Australia: evidence for two distinctive events of mafic magmatism and crustal extension. *Chem. Geol.* 109, 341–354.
- Zhou, M.F., Kennedy, A.K., Sun, M., Malpas, J., Leshner, C.M., 2002a. Neoproterozoic arc-related mafic intrusions along the northern margin of South China: implications for the accretion of Rodinia. *J. Geol.* 110, 611–618.
- Zhou, M.F., Ma, Y.X., Yan, D.P., Xia, X.P., Zhao, J.H., Sun, M., 2006a. The Yanbian terrane (southern Sichuan Province, SW China): a Neoproterozoic arc assemblage in the western margin of the Yangtze Block. *Precambrian Res.* 144, 19–38.
- Zhou, M.F., Yan, D.P., Kennedy, A.K., Li, Y., Ding, J., 2002b. SHRIMP U–Pb zircon geochronological and geochemical evidence for Neoproterozoic arc-magmatism along the western margin of the Yangtze Block, South China. *Earth Planet. Sci. Lett.* 196, 51–67.
- Zhou, M.F., Yan, D.P., Wang, C.L., Qi, L., Kennedy, A., 2006b. Subduction-related origin of the 750 Ma Xuelongbao adakitic complex (Sichuan Province, China): implications for the tectonic setting of the giant Neoproterozoic magmatic event in South China. *Earth Planet. Sci. Lett.* 248, 271–285.
- Zhou, M.F., Zhao, J.H., Xia, X.P., Sun, W.H., Yan, D.P., 2007. Comment on “Revisiting the ‘Yanbian Terrane’: implications for Neoproterozoic tectonic evolution of the western Yangtze Block, South China” [*Precambrian Res.* 151 (2006) 14–30]. *Precambrian Res.* 155, 313–317.
- Zhu, W.G., Liu, B.G., Deng, H.L., Zhong, H., Li, C.Y., Pi, D.H., Li, Z.D., Qin, Y., 2004. Advance in the study of Neoproterozoic mafic–ultramafic rocks in the western margin of the Yangtze Craton. *Bull. Mineral. Petrol. Geochem.* 23, 255–263 (in Chinese).
- Zhu, W.G., Zhong, H., Deng, H.L., Wilson, A.H., Liu, B.G., Li, C.Y., Qin, Y., 2006. SHRIMP zircon U–Pb age, geochemistry and Nd–Sr isotopes of the Gaojiacun mafic–ultramafic intrusive complex, SW China. *Int. Geol. Rev.* 48, 650–668.
- Zhu, W.G., Zhong, H., Li, X.H., Liu, B.G., Deng, H.L., Qin, Y., 2007. ^{40}Ar – ^{39}Ar age, geochemistry and Sr–Nd–Pb isotopes of the Neoproterozoic Lengshuiqing Cu–Ni sulfide-bearing mafic–ultramafic complex, SW China. *Precambrian Res.* 155, 98–124.